December 2019

Microfabricated Substrate to Achieve In Vivo-Like Cardiomyocyte Morphology and Electrical Propagation in Neonatal Cell Culture

Tiffany Yu
Clemson University, tiffanyyu3230@yahoo.com

MICROFABRICATED SUBSTRATE TO ACHIEVE IN VIVO-LIKE CARDIOMYOCYTE MORPHOLOGY AND ELECTRICAL PROPAGATION IN NEONATAL CELL CULTURE

A Thesis
Presented to
the Graduate School of
Clemson University

In Partial Fulfillment
of the Requirements for the Degree
Master of Science
Bioengineering

---

by
Tiffany Chin Yu
December 2019

Accepted by:
Dr. Zhi Gao, Committee Chair
Dr. Delphine Dean
Dr. William Richardson

ABSTRACT

Because of the complexity of the *in vivo* environment, much physiological and pathological understanding of the human body is obtained through cell culture. To gain clinically relevant knowledge, having a cell culture model that mimics the corresponding *in vivo* tissue would be advantageous. For example, when studying the mechanical and electrical coupling between cardiac cells, imitating *in vivo* cellular morphology correlates with improved electrical coupling. This has applications within drug screening; by being able to test for cardiotoxicity with a cell culture model, this reduces the resources needed to screen pharmaceuticals for negative side effects.

In conventional cardiomyocyte culture, cells spread randomly and express irregular, star-like morphology without forming *in vivo*-like structures. The purpose of this aim was to utilize microfabricated features such as wrinkles on polydimethylsiloxane (PDMS) and examine the effects of substrate topography on cardiomyocyte morphology and function. Of the substrate topographical parameters that result in optimal cellular alignment, we evaluate the electrical cohesiveness of these cell culture models via cellular calcium transients.

Mammalian cardiomyocytes use the calcium-induced calcium release (CICR) pathway to induce calcium transients that are integral to the excitation-contraction cycle. Their efficiency in this is an indication of their electrophysiological maturity. Due to the intimate dynamics between physical and functional maturity, we examined how substrate

topography affects the ability of cultured neonatal cardiomyocytes to cycle calcium ions in response to external stimulation.

ACKNOWLEDGEMENTS

I would like to thank my advisor Dr. Bruce Zhi Gao for all of his help and mentorship through the duration of my graduate studies; I could not have progressed my research without his guidance. I would also like to express appreciation to my other committee members, Dr. Delphine Dean and Dr. William Richardson, for their guidance along my research path. Thank you to Clemson Godney-Snell Research Center for providing neonatal rats weekly; Jonathan Haywood and Patricia Tate of Dr. Richardson's lab for their aid in cell harvesting and isolation; Dr. Tyler Harvey and Dr. Vladmir Reukov for their invaluable help in AFM scanning; Lucas Schmidt for his aid in mechanoelectrical and imaging systems; Ailin Wei and Xiaoqi Yang for assistance in cell culture and analysis protocol; Adam Baker and Reece Fratus for managing the lab efficiently; Shenghao Tan for his help in streamlining the stretch release machine system; Maria Torres and Trish Nigro for their help with clarifying my academic and professional pathways.

Finally, I would like to express gratitude for the Clemson University Department of Bioengineering for providing me the opportunity to expand my horizons and pursue higher education. This research was funded by NIH grant R01HL144927.

TABLE OF CONTENTS

Page

Table of Contents (Continued) Page

LIST OF TABLES

Table Page

LIST OF FIGURES

List of Figures (continued)

Figure Page

LIST OF GRAPHS

Graph Page

CHAPTER 1

INTRODUCTION

Cardiotoxicity is a critical issue regarding the pharmaceutical industry – even noncardiac drugs can have drastically negative cardiac side effects. Even drugs deemed safe and effective in animal models can manifest as cardiotoxic effects in human patients. Up to ninety percent of pharmaceuticals that pass the pre-clinical phase do not successfully pass the clinical phase (Kane, Couch, & Terracciano, 2015). Thus, developing an accurate preclinical assessment of pharmaceuticals is of utmost importance in the biotechnology industry.

Significance

Cardiotoxicity can be exhibited in different manners, but one of the most common effects associated with drugs is a specific type of ventricular tachyarrhythmia known as Torsades de pointes (TdP), where the QT interval of an electrocardiogram (ECG) is prolonged; the QT interval is when the heart ventricles electrically depolarize and repolarize, leading to contraction abnormalities and delaying the heartbeat (Fermini & Fossa, 2003; Mummery et al., 2012). TdP is the second most leading reason for approved pharmaceuticals on the market being withdrawn; despite this, most drugs identified with QT prolonging side effects are only (Fermini & Fossa, 2003; Natarajan et al., 2011). Over the past 40 years, cardiotoxicity is the leading cause of drug withdrawals within the United States market; half of these situations are due to arrhythmias such as TdP (Mandenius et al., 2011; Piccini et al., 2009). The International Council on

Harmonization of Technical Requirements for Pharmaceuticals for Human Use (ICH) has guidelines for 'Safety Pharmacology Studies for Human Pharmaceuticals', where section S7A focuses on testing electrophysiology *in vitro* and *in vivo* (Mandenius et al., 2011). Recent cancer treatment drugs have in particular had unexpected cardiac side effects that need improved drug screening approaches (Kurokawa & George, 2016).

While stem cell-derived cardiomyocytes have many potentials, they currently still have limited maturation potential. Both embryonic and induced pluripotent stem cell derived-cardiomyocytes have shown inadequacy of function compared to primary neonatal ones, themselves having limited functionality compared to adult cardiomyocytes (Knight et al., 2015).

It is well known that typically, animal models are used for pre-clinical drug screenings; pharmaceutical products must pass these studies before the FDA allows advancement to clinical trials, using human patients. However, these do not precisely reproduce how the human heart would respond to tested drugs. There are existing in vitro assays that have become standards in drug screening uses, but these do not fully capture the behavior of in vivo cardiomyocytes and can overlook cardiotoxicity; this leads to undesirably high rates of failure during clinical trial phases that cause unnecessary endangerment to the tested patients and increases costs (Kurokawa & George, 2016; Mathur, Ma, Loskill, Jeeawoody, & Healy, 2016). Thus, these is a need to create an in vitro drug screening model that fully captures the mechanical, electrical, and thus functional properties of native cardiac tissue, to imitate the actual pharmacological effects of tested drugs.

Mature cardiomyocytes cannot be utilized in drug testing models because of their shortcomings in proliferation, viability, and uncontrollable variation (Dick, Rajamohan, Ronksley, & Denning, 2010). They are minimally proliferative; because of this, when parts of the myocardium scar due to issues such as myocardial infarction, the body is not able to regenerate fully functional cells to replace the ones that die (Knight, Grosberg, & McCain, 2015).

The cardiac microenvironment in vivo is very complex; while desirable to create an in vitro system mimicking this fully, it is much more feasible and sensible to focus on recreating the myocardium, where most force generation and electrical propagation occurs (Kurokawa & George, 2016).

Once such strategies become available, there is promise that plausible cardiac drug testing models could become more relevant and usable by the exploration of this approach. This contribution is significant for pre-clinical drug testing to ensure safety and efficacy before proceeding to clinical trials. Thus, important advances in physiologically accurate drug testing models could be expected. In addition, the research will be of significance because it will contribute to a broader understanding of cardiac cell physiology.

This contribution is significant because it is expected to lead to the development of a safe and effaceable cardiac drug testing model that will allow for a physiologically accurate approach to reduce use of animal models before clinical trials as well as screening out pharmaceuticals with cardiotoxicity risks.

Objectives

The overall goal is to better understand how different parameters of an engineered substrate will enhance in vivo-like cardiac cell culture model morphologically and functionally. If successful creation of repeatable cardiac cell cultures can be made, this is a step closer to creating a model in which drug testing uses are plausible, reducing use of animal models. Thus, there is a critical need for the establishment of a standard substrate fabrication protocol to culture cardiomyocytes in a manner that would be suitable for drug testing models.

Little is known about how substrate topography affects the functionality and morphology of cardiomyocyte development, though extensive research has pursued using the substrate to encourage longitudinal alignment of cardiomyocytes.

Therefore, the aims of this work are intended to address these knowledge gaps in our understanding of cardiomyocyte morphology and its influence on cardiac electrophysiology. To fill in these voids of knowledge, we will customize the mechanical parameters of the substrates used in our cardiac cell culture model to answer these key questions.

With the completion of this work and moving forward, we achieve enhanced understanding of the influence of substrate topography on the morphology and functionality of cardiomyocytes. The substrate parameters that result in satisfactory cardiomyocyte morphology will be examined functionally in more detail; cellular electrophysiology will be analyzed by observing cellular calcium cycling.

References

Dick, E., Rajamohan, D., Ronksley, J., & Denning, C. (2010). Evaluating the utility of cardiomyocytes from human pluripotent stem cells for drug screening. *Biochemical Society Transactions*, *38*(4), 1037–1045. https://doi.org/10.1042/BST0381037

Fermini, B., & Fossa, A. A. (2003). The impact of drug-induced QT interval prolongation on drug discovery and development. *Nature Reviews Drug Discovery*, *2*(6), 439–447. https://doi.org/10.1038/nrd1108

Kane, C., Couch, L., & Terracciano, C. M. (2015). Excitation – contraction coupling of human induced pluripotent stem cell-derived cardiomyocytes. *Frontiers in Cell and Developmental Biology*, *3*, 1–8. https://doi.org/10.3389/fcell.2015.00059

Knight, M. B., Grosberg, A., & McCain, M. L. (2015). In Vitro Tools for Quantifying Structure - Function Relationships in Cardiac Myocyte Cells and Tissues. In *Cardiac Cytoarchitecture: How to Maintain a Working Heart* (pp. 15–39). Springer International Publishing. https://doi.org/10.1007/978-3-319-15263-9

Kurokawa, Y. K., & George, S. C. (2016). Tissue engineering the cardiac microenvironment: Multicellular microphysiological systems for drug screening. *Advanced Drug Delivery Reviews*, *96*, 225–233. https://doi.org/10.1016/j.addr.2015.07.004

Mandenius, C. F., Steel, D., Noor, F., Meyer, T., Heinzle, E., Asp, J., … Sartipy, P. (2011). Cardiotoxicity testing using pluripotent stem cell-derived human cardiomyocytes and state-of-the-art bioanalytics: A review. *Journal of Applied Toxicology*, *31*(3), 191–205. https://doi.org/10.1002/jat.1663

Mathur, A., Ma, Z., Loskill, P., Jeeawoody, S., & Healy, K. E. (2016). In vitro cardiac tissue models: Current status and future prospects. *Advanced Drug Delivery Reviews*, *96*, 203–213. https://doi.org/10.1016/j.addr.2015.09.011

Mummery, C. L., Zhang, J., Ng, E. S., Elliott, D. A., Elefanty, A. G., & Kamp, T. J. (2012). Differentiation of human embryonic stem cells and induced pluripotent stem cells to cardiomyocytes: A methods overview. *Circulation Research*, *111*(3), 344–358. https://doi.org/10.1161/CIRCRESAHA.110.227512

Natarajan, A., Stancescu, M., Dhir, V., Armstrong, C., Sommerhage, F., Hickman, J. J., & Molnar, P. (2011). Patterned cardiomyocytes on microelectrode arrays as a functional, high information content drug screening platform. *Biomaterials*, *32*(18), 4267–4274. https://doi.org/10.1016/j.biomaterials.2010.12.022

Piccini, J. P., Whellan, D. J., Berridge, B. R., Finkle, J. K., Pettit, S. D., Stockbridge, N., … Krucoff, M. W. (2009). Current challenges in the evaluation of cardiac safety during drug development: Translational medicine meets the Critical Path Initiative. *American Heart Journal*, *158*(3), 317–326. https://doi.org/10.1016/j.ahj.2009.06.007

CHAPTER 2

DETERMINING THE MECHANICAL PROPERTIES OF THE WRINKLED SUBSTRATE REQUIRED FOR THE FORMATION OF IN VIVO-LIKE CARDIOMYOCYTE MORPHOLOGY IN NEONATAL CULTURE

Cardiovascular diseases are the leading source of deaths worldwide, causing approximately one third of deaths in the United States (Besser et al., 2018). Heart muscle damage usually results from myocardial infarction, resulting in scar damage that affects the functionality of the adult heart; this means that the electrical signals that trigger synchronized contractions get disrupted, in itself leading to further heart failure (Zheng et al., 2012). Thus, it is of utmost importance to be able to imitate *in vivo* parameters in order to achieve *in vitro* culture that is functionally accurate and comparable to cells within the body. To do so, we need to be able to define the unique environment in which cardiomyocytes reside in and emulate these elements.

Introduction

Cardiovascular System

The cardiovascular system exists within an organism to allow transport of fluids and nutrients as needed throughout the body via blood. The heart beats with enough force to pump oxygenated blood out of through vasculature to reach every part of the body; simultaneously, deoxygenated blood returns to the heart for oxygenation and the cycle runs again.

Heart

The heart has four chambers – two upper atriums and two lower ventricles. The overall heart has three layers – the endocardium, the myocardium, and the epicardium, from the outside in; the myocardium makes up the bulk of the heart, providing the strength via contraction to push oxygenated blood out to the body. On a cellular level, the myocardium is primarily made up of two types of mature cells: cardiomyocytes, the electrically excitable muscle cells that contract, and fibroblasts, the cells that synthesize and maintain the extracellular matrix (ECM). While cardiomyocytes comprise a larger volume of the myocardium, fibroblasts are larger in numbers (Simmons, Petzold, & Pruitt, 2012). Cardiomyocytes are estimated to take up 75% of volume but comprise 40% of cell count – the others are fibroblasts and trace amounts of vascular endothelial smooth muscle cells (Acosta-torres, Bax, Spreeuwel, & Bouten, 2013) and

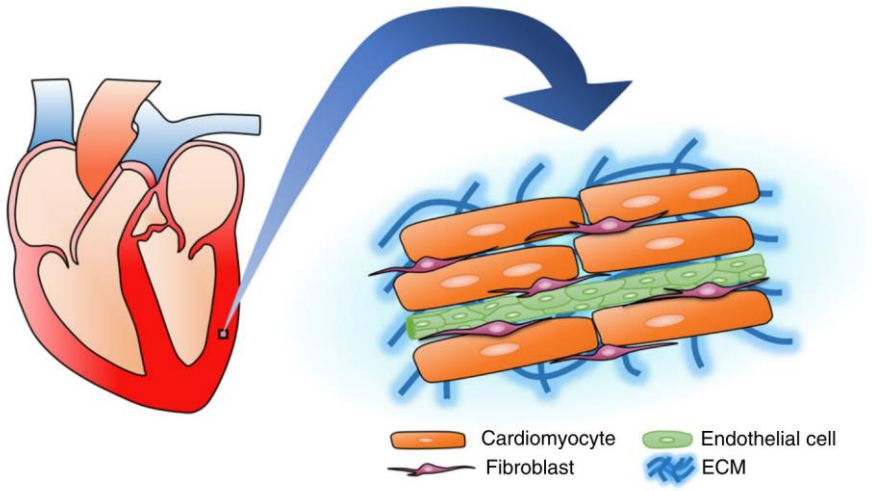

Figure 2.1: Cardiomyocytes and other cells within the heart in vivo (Reprinted with permission from Kurokawa 2016)

Ventricular Cardiomyocytes

The ventricles are comprised of muscle cells called ventricular cardiomyocytes that are particularly responsive to electrical excitability, layered densely to make up cardiac tissue. The collective effort of these individual cells create enough force to contract the heart, mobilizing a high volume of blood within the body. Although individual cells vary in size, they have a fairly consistent length-to-width ratio, being 100-150 μm long and 10-20 μm wide (Kleber & Rudy, 2004; Macfarlane et al., 2010; Veeraraghava, Gourdie, & Poelzing, 2014).

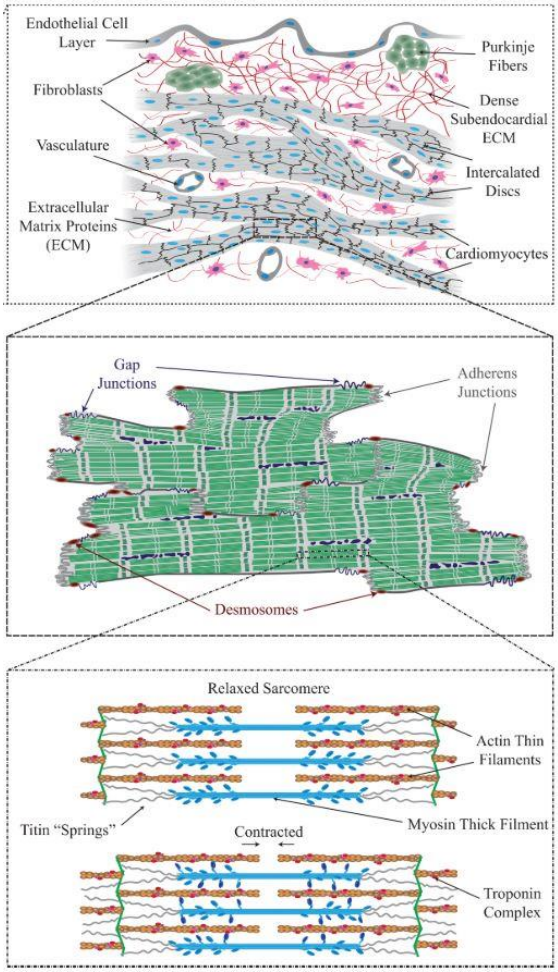

Figure 2.2: Cardiomyocyte structure within cardiac tissue and sarcomere structure within cardiomyocyte (Reprinted with permission from Simmons 2012)

Intercalated Disc

Cardiomyocytes are connected to each other via junctions along the cellular interfaces. The most prominent of these are intercalated discs, which are the longitudinal end-to-end connections between the cardiomyocytes. These are made of desmosomes, fascia adherens, and gap junctions, the primary elements that support its role; there are over 200 other proteins to assist, such as ion channels, scaffolding proteins, signaling molecules (Manring, Dorn, Ex-willey, Accornero, & Ackermann, 2018). Desmosomes and fascia adherens are the mechanical junctions that provide mechanical integration and strength to these interfaces; desmosomes attach cell membranes to the structural network within the cell, to withstand physical stresses put upon the cells;, while fascia adherens anchor the cell membrane to the actin cytoskeleton and allow for the transferal of contractile forces (Manring et al., 2018; Noorman et al., 2009; Sheikh, F., Ross, R.S., and Chen, 2009). In contrast, gap junctions are the channels that allow for electrical impulses to propagate through connecting cells, thus allowing for electrical stimulation and contraction of the cardiomyocytes. The gap junctions are essential to the functionality of cardiomyocytes because of their electrical nature and ties in with the ability of the heart to contract efficiently. However, these proteins with different functions have symbiotic relationships; for example, desmocollin, which is a type of cadherin, directly interacts with Cx43 to give it support (Manring et al., 2018).

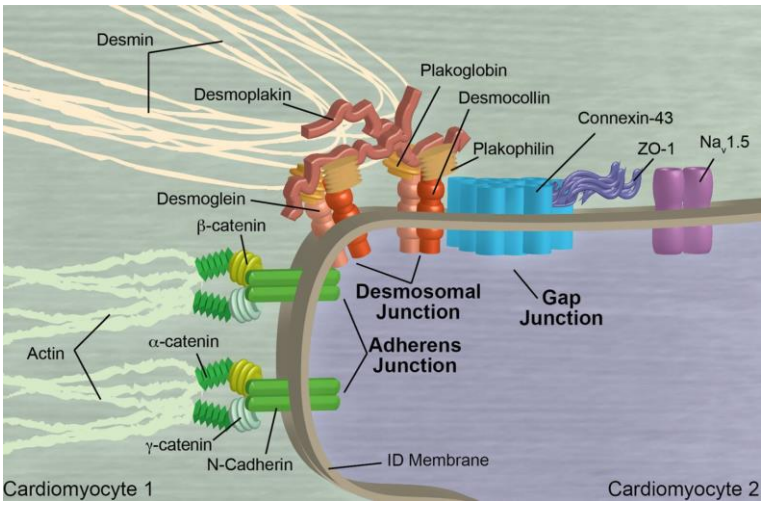

Figure 2.3: Structures within the intercalated disc of cardiomyocytes (Reprinted with permission from Manring 2018)

Gap Junctions

Gap junctions are mostly concentrated at the longitudinal ends of adult cardiomyocytes, where the intercalated disks allow for communication between cells. Gap junctional proteins, known as connexins, form the intermembrane channels between cardiomyocytes to transport small molecules (smaller than 1000 Daltons), nutrients, and ions; six of these units congregate to form a single gap junction (Sigg, Laizzo, Xiao, & He, 2010).

Literature Review

Murine Neonatal Cardiomyocytes

Although the cell sources commonly used in cardiovascular biomedical research vary across several species, for our purposes we are utilizing neonatal cardiomyocytes from murine sources. These are beneficial because they are immature, and able to be cultured *in vitro* without difficulty; at the same time, they are already fully differentiated

into the correct lineage and have low proliferation (Luna et al., 2011; Sigg et al., 2010). Because they're primary cells, the cardiac ion channels are already assembled, and channel ratios of human cardiomyocytes are similar to many mammalian ones used for electrophysiology studies, and are already well established for studying drug toxicity (Chlopčíková, Psotová, & Miketová, 2001; Mandenius et al., 2011). Murine sources are also optimal because they are thoroughly characterized for research purposes, and are straightforward to grow in large quantities (Zimmermann et al., 2000). From a cell culture perspective, these have a relatively simple isolation procedure compared to adult cardiomyocytes, which are sensitive to calcium concentration within the medium (Chlopčíková et al., 2001).

Ventricular cardiomyocytes are the only cardiomyocytes that form T-tubules, which are important for calcium cycling and electrical synchronization; they are not present in atrial myocytes, which will be relevant for Aim 2 (Später, Hansson, Zangi, & Chien, 2014). Ventricular myocyte action potential is closely associated with the QT interval on an ECG, so these are optimal for studying prolongation (Sigg et al., 2010).

An ideally matured cardiomyocyte cell culture will have certain characteristics, including clearly organized sarcomere structures, extracellular matrix surrounding the cells, and well established cellular junctions (Soares et al., 2012).

Extracellular Matrix

Cells are held together by extracellular matrix (ECM), a complex network of molecules such as polysaccharides, proteins, cytokines, and growth factors; these have

a wide variety of compositions throughout the body, modified to best provide biochemical and mechanical support to the cells in question (Saini, Sam, Kharaziha, & Nikkhah, 2015).

Cardiomyocytes are surrounded by ECM, fabricated and rearranged by cardiac fibroblasts; this ECM mainly supplies elasticity to the cardiac tissue to optimize the contractility of the cardiac cells. The extracellular matrix is comprised of a wide variety of proteins; this ranges from fibrous proteins like collagen and elastin, bringing mechanical stability to the table, to adhesion proteins such as fibronectin and laminin that secure cells to the ECM. These fibers are naturally heterogeneous in arrangement and thickness *in vivo* (US 9.452,564 B2, 2016).

ECM micro- and nano-level features heavily influence cellular morphology, adhesion, and growth. Myocardial ECM has aligned fibrils that are as small as about 100 nanometers in diameter; this nanotopography increases the surface area upon which cells can attach and absorb proteins from (Martínez, Engel, Planell, & Samitier, 2009). The collagen fibers that bundle cardiomyocytes together (perimysium) have fiber clusters between 0.5-10 μm in diameter and spaced between 100-200 μm apart; these fibers also orient parallel with the cardiac muscle longitudinal axis and thus also influence alignment and functionality (Mathur, Ma, Loskill, Jeeawoody, & Healy, 2016).

Elastic Substrate Types

Cardiomyocytes cannot simply be cultured on a hard, flat surface, such as a petri dish; this does not allow for the biomechanical and biochemical cues of the cells to

allow for correct alignment and morphology (P. Y. Wang, Yu, & Tsai, 2010). These cultures are also at risk for dedifferentiating due to a lack of microenvironmental cues, reverting back to star and oval morphology (Au, Cui, Chu, Veres, & Radisic, 2009). On a microscopically flat surface, the myofibrils are not organized well and intercellular junctions don't form, preventing the transmission of electrical signals through long series of cells (McDevitt et al., 2002). Thus, the in vitro substrate must have elastic characteristics to encourage the cells to culture with an *in vivo*-like morphology and thus functionality.

There is a wide array of substrates with elastic mechanical characteristics that are good choices to be considered. Popular materials used for cardiac cell cultures include polystyrene (PS), poly(methylmethacrylate) (PMMA), and poly-ether-urethane (PU) (Martínez et al., 2009). However, PDMS has been chosen as the optimal substrate, because of its elastic tunability, low costs, and nontoxicity to cells; features on the nano-scale can also be made on PDMS (George, 2014). PDMS also is transparent and allows for high elongation (200%) before fracture, making it an advantageous choice for our purposes (Nania, Matar, & Cabral, 2015).

Substrate Fabrication Methods

Fabricating patterns onto materials at a microscopic level has been used in multiple applications in the scientific world, ranging from leaf beetle traction to phage-displayed peptide patterning (Swaminathan, Bullough, Li, Zhou, & Cui, 2013; Voigt, Schweikart, Fery, & Gorb, 2012). They have been especially useful in electronic and

biological applications, where precision to a diminutive degree affects outcomes greatly. One such biological application involves taking advantage of micropatterning to mimic the native physical environment of cells *in vivo* by transferring these parameters *in vitro*. For cardiomyocytes, which do not proliferate *in vitro* and have geometries specific and unique to their cell type, it is crucial to closely imitate the *in vivo* environment to maximize viability in culture.

This is where microfabrication becomes relevant. By examining the mechanical nature of native ECM, we can imitate this using other materials and optimize the ability to culture cardiomyocytes *in vivo*.

Topographical and mechanical cues are essential to both cardiomyocyte and heart development, which are interconnected. Studies have shown that during embryonic heart tube growth, the tube bends roughly into the heart shape even when not within an embryonic environment, indicating an intrinsic mechanism of actin filament growth that flattens cells only on the convex side to induce the initial fold, showing that cellular changes lead to morphology changes anatomically (McCain & Parker, 2011). The native heart has a heterogeneous ECM topography, influenced by elements such as nerves, blood vessels, and fibrotic tissue; thus, these also influence how the cytoskeleton is organized and restructured, and thus the overall morphology of the cell (McCain & Parker, 2011). Cells *in vitro* have been shown to have a positive feedback system with the ECM that they fabricate, reflecting likely occurs *in vivo*. when cells secrete their own ECM, the ECM proteins have fibrils that align with the cells themselves, which further encourage the directionality of the cells themselves and neighboring cells also, creating a

cascade effect of alignment and morphology (Carson et al., 2016). Thus, fabricated substrate must be designed to mimic the topography of the cell's natural environment within ECM.

Different microfabrication methods, such microcontact printing and photolithography, have been the gold standard in aligning cells in an in vivo-like manner. Microprinting involves adding adhesive proteins such as fibronectin, laminin, and collagen in an ordered manner on a micro scale to a flat substrate, to encourage cellular alignment; photolithography is creating micropatterns of adhesion using ultraviolet (UV) light and photoresist (Yap & Zhang, 2007).

Although these are more successful than electrical cues, these only yield mechanical features on the scale of 10s to 100s of microns; this indicates that heart tissue may be responsive to smaller features as well. Microscale mechanical features with softer contours cause cells to react much more like native tissue than the hard microgroove edges, causing directional alignment of ECM fibers such as fibronectin that further align the cells themselves (Bae et al., 2015; Hu et al., 2014).

Substrate Nanofabrication Methods

There are currently nanofabrication methods such as nanoimprint lithography and electron beam lithography to create such features; however, these are costly and difficult procedures. Thus, microfabricating multiscale wrinkles on an elastic substrate is an optimal solution. This procedure is relatively fast, inexpensive, and strong; additionally, it is able to create microscale and nanoscale features simultaneously, making the

substrate suitable for cardiomyocyte alignment (Luna et al., 2011). Compared to photolithography methods, wrinkling the membrane creates rounded edges, thus along for gradient formation (Jiang et al., 2002). This approach is optimal to microgrooves because of the elimination of sharp angles as well as flat surfaces that limit intercellular communication; a study found that wrinkles resulted in higher alignment and adhesion strength as well as lower death rates of cells compared to microgrooves (Carson, D., Hnilova, M., Yan, X., 2016; Hu et al., 2014).

Wrinkles

Wrinkles in Cellular Applications

Wrinkles have been examined closely in within the scientific community for a multitude of purposes. For example, wrinkled PDMS has been for everything from examining the attachment of leaf beetles to the patterning of viruses (Swaminathan et al., 2013; Voigt et al., 2012). This is because nature has no hard lines; rather, soft contours exist across the spectrum. Thus, scientists have accordingly attempted to recreate this in biological applications. This approach has been particularly popular when applying to cellular research, because cells respond to mechanical cues of their environment. For instance, bovine capillary endothelial cells were cultured on wrinkled PDMS to encourage the extent of their spreading; the authors proposed that waves lack the sharp angles of the traditional microgroove topography, allowing for the cells to respond to an environment with more native characteristics (Jiang et al., 2002). Similarly, another study examined bovine aortic endothelial cells cultured on wrinkled PDMS and micro-

grooved PDMS with similar topographical features sizes except for the rounded versus squared edges; they found that with all other variables held constant, the waved PDMS pattern resulted in more alignment and less cell death than the microgrooves (Hu et al., 2014).

Wrinkles in Cardiomyocyte Alignment Applications

Wrinkled elastic substrates are especially applicable in cardiomyocyte cell cultures, because of their inherently longitudinal morphology in the native environment. In one instance, neonatal rat cardiomyocytes were cultured on wrinkled PDMS, formed by a mold, and inspected for alignment; they found that cells cultured on the wrinkles were much more aligned than those cultured on a flat substrate control, and that the localization of gap junctional proteins matched accordingly (Luna et al., 2011). They also repeated the experiment with isolated human embryonic stem cell-derived cardiomyocytes with the same results – wrinkles strongly influence cell alignment (Luna et al., 2011).

Wrinkle Fabrication Methods

Having substrate features that are too large will result in the cells lacking sufficient contact area to communicate with substrate cues; on the other hand, having wrinkles that are too narrow will result in limited cell contact as well because the cells cannot fully penetrate the contours (D. H. Kim et al., 2010).

Several methods of fabricating hierarchical wrinkles on PDMS currently exist. The most common ones are layer deposition onto the PDMS, ultraviolet (UV) radiation,

oxygen-plasma treatment, electrical discharge, and ion beam (Cao, Chan, Zang, Leong, & Zhao, 2014; Lin, Zhang, Lv, Tang, & Yin, 2018; Wei & Zhao, 2014). These processes all cause the Si-CH_3 groups on the exposes surface to be cleaved into SiO_x groups, or replacing methyl groups with silanol ones; this makes the surface tough, dense, and amorphous (Bhattacharya, Datta, Berg, & Gangopadhyay, 2014; Nania et al., 2015). This causes the surface to become hydrophilic, lowering the contact angle of water (Bhattacharya et al., 2014). With the release of a pre-set strain on the PDMS membranes, the difference between the brittle oxidized top layer and the softer remainder of the substrate will result in the surface buckling, creating wrinkles; the difference in Poisson ratio and elastic modulus of these two layers cause wrinkles upon stress relaxation (Rodríguez-Hernández, 2015). While all these variations of multiscale wrinkle fabrication have merit in creating consistent, quantifiable topographical elements, there are limitations in accessible machinery. Given resources available, the two methods tested will be UV-ozone and oxygen-plasma treatment. In theory, using these two methods can create wrinkles anywhere from 150 nm to hundreds of microns (Rodríguez-Hernández, 2015).

UV-ozone treatment

The PDMS substrate is held at a certain strain, and undergoes UV-ozone treatment to chemically change the surface to silica; under this mixture of treatment, silicone polymers become more hydrophilic, but also stiffer at the surface (Efimenko, Wallace, & Genzer, 2002; Rodriguez-Hernandez, 2015). Following UV-ozone treatment, the substrate will be released back to zero strain at set, specific rates, as controlled by the

custom-built strain release device. Because of the difference between the stiffer surface and soft substrate, this release will cause the surface of the substrate to buckle, forming wrinkles (Campo, 2015; Efimenko et al., 2005).

Oxygen-plasma treatment

To create wrinkles using this method, similar to the UV-ozone treatment, the PDMS is also held at a certain strain under treatment conditions to allow for silica formation on the surface of the substrate (Bowden, Huck, Paul, & Whitesides, 1999; Mei, Kiravittaya, Harazim, & Schmidt, 2010; Moon & Vaziri, 2009; Swaminathan et al., 2013). However, the treatment process is different. The substrate will be isolated in a vacuum chamber to allow for the creation of plasma; once at a low enough pressure, oxygen gas is allowed into the chamber simultaneously with the formation of plasma, initiating the chemical changes on the surface. This will be allowed to cool (the treatment heats up the substrate), and then the strain will be released at the same rates using the strain release device to create buckling of the surface. Bowden et al. indicates that the key parameter for influencing wavelength and amplitude of the wrinkles will be the PDMS temperature and oxidation duration; they were able to create wavelengths between 0.5 and 10 μm. Increasing oxidation time correlates with a larger wrinkle wavelength and amplitude (Mei et al., 2010). Plasma treatment causes the surface of the PDMS to have increased presence of polar functional groups such as silanol (SiOH) that increases hydrophilicity of the surface, changing the water contact angle from 120° to a range of 17-46° depending on plasma treatment time (Tan, Nguyen, & Chua, 2010). It

can also cause nanocracks to form on the surface, increasing RMS roughness; however, these nanocracks can increase cell attachment with the addition of adhesive proteins (Tan et al., 2010).

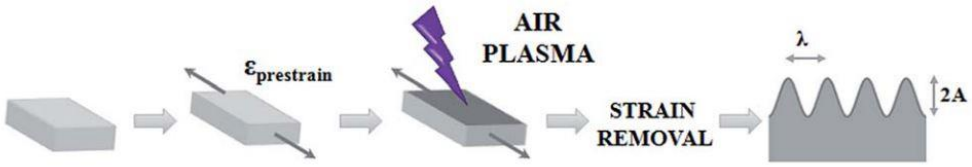

Figure 2.4: Steps for inducing wrinkles in elastic substrate using air plasma (Reprinted with permission from Nania 2015)

Parameters of Wrinkle Fabrication

With both plasma and UV-ozone treatment, there are several parameters that alter the topography of the resulting wrinkles. This includes treatment time, strain, release rate, temperature, uniaxial versus biaxial strain, and gas composition.

Another aspect relevant to the wrinkle topography when using plasma is the pressure within the treatment chamber. There is a threshold pressure at which any lower values will not allow for plasma ignition, based on Pashen's law; one study found that their threshold pressure was 1 mbar (Nania et al., 2015). They also found that increasing chamber pressure during plasma treatment results in smaller wrinkle wavelength with other variables unchanged. This is because higher pressure slows down oxidation kinetics that form the oxidized layer, thus making it thinner and reducing wavelength (Nania et al., 2015).

The plasma dose, or intensity of the plasma created, also influenced the wrinkles. Nania et al (2015) found that there is a logarithmic relationship between both amplitude and wavelength with plasma dose. We will be keeping the gas composition, pressure, and strain constant as well as a uniaxial strain, while changing plasma treatment time and stretch release rate.

Multiscale Wrinkle Development

Some research groups have taken the approach of using a two-step treatment process to generate multiscale wrinkles. Cao et al. combined plasma and UV-ozone to treat PDMS surfaces. They used a set strain and treated this with oxygen plasma, partially released the strain to create nano-scale wrinkles; they then did a second treatment with UV-ozone followed by full release of the strain to cause buckling on a larger, micro-scale.

On the other hand, it is possible to create them using just one step. Efimenko et al. (2005) created wrinkles using a single-step UV-ozone treatment; they were able to create hierarchal wrinkles ranging five orders of magnitude, ranging from a few nanometers to nearly a millimeter in wavelength.

Materials and Methods

Wrinkled Membrane Fabrication

The flat untreated membranes are created using Sylgard 184 Silicone Encapsulant (Dow Corning, Midland, MI), at the standard 10:1 base-to-crosslinker ratio, to keep the

Young's Modulus constant. The thickness of the membranes are kept constant, by spinning freshly prepared, room temperature PDMS at 200 rpm for 1 minute using Model WS-400B-6NPP/LITE Spin Coater (Laurell Technologies Corporation, North Wales, PA) on 100 mm silicon wafers (University Wafer, Inc., South Boston, MA) then baking at 95°C for 1 hour to complete the cross-linkage. These are stored in 100% EtOH to remove unlinked polymers until further use.

Pre-stretched PDMS membrane was treated with UV-Ozone and released, with no perceivable wrinkles created. The Novascan PDS Series UV-Ozone machine (Novascan Technologies, Inc., Boone, IN) was set at the highest settings at varying times of treatment with no changes in results, indicating that the strength was most likely not enough to fully oxidize and harden the top surface.

The wrinkles are created using the strain, air-plasma treatment time, and stretch release rate as the variables. For our purposes, the pressure, plasma dose, and unwrinkled membrane thickness will be kept constant. Pressure is lowered to 400 mTorr before initiating plasma formation. Samples of the pre-prepared PDMS membranes are measured to confirm consistent thickness. They are then pre-stretched manually on a custom-made stretch device to various strains before the air-plasma treatment. The device loaded with the PDMS membrane will then be placed in the plasma cleaner (Harrick Plasma, Ithaca, NY), which is then connected to the vacuum pump (Varian Vacuum Technologies, Lexington, MA) to allow for the pressure reduction required to produce plasma. The plasma power setting is kept at the high switch level of 29.6 W.

After treatment, the stretch release device will be loaded onto a motor-driven custom-designed assembly to carefully release the PDMS strain at a controlled rate.

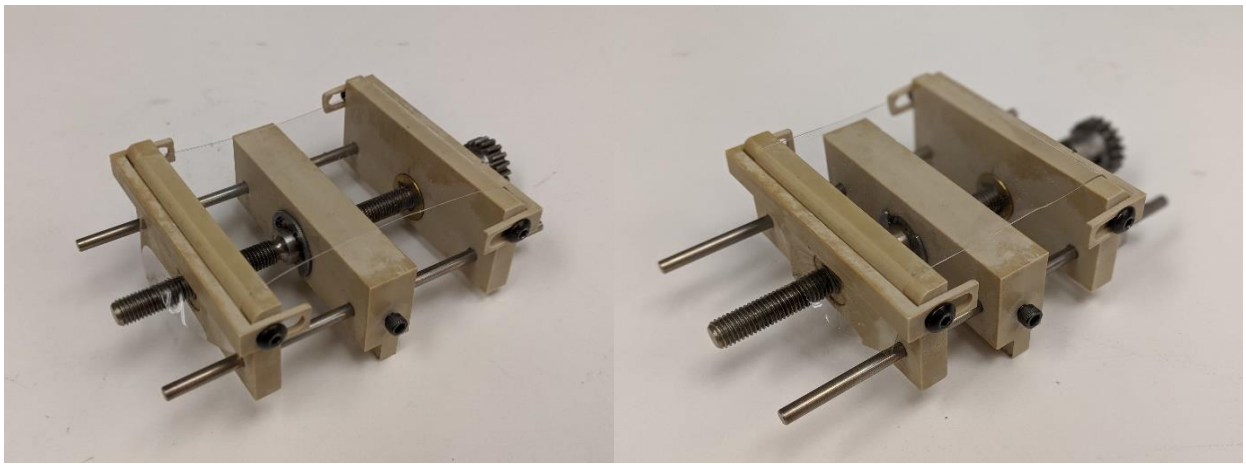

Figure 2.5: PDMS in custom built stretch release device before plasma treatment (Left): Stretched (Right): Without stretch

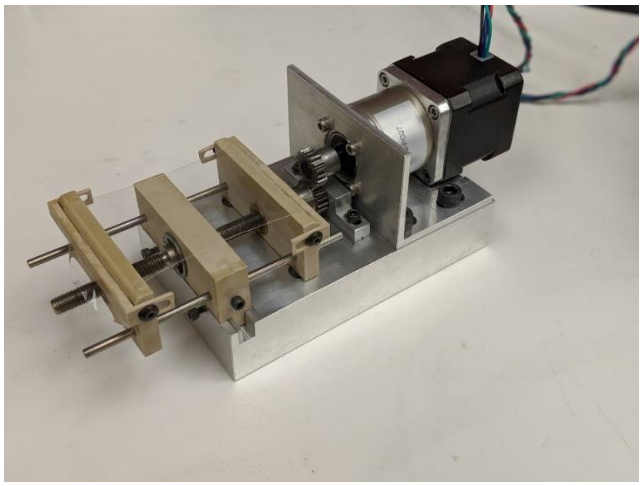

Figure 2.6: Stretch release device with PDMS. PDMS inserted into apparatus that allows for constant release of strain, creating wrinkles.

Wrinkled Membrane Characterization

The post-treated PDMS will be analyzed using atomic force microscopy (AFM) (Asylum Research AFM, Santa Barbara, CA) to quantify the wavelengths and amplitudes of these

wrinkles. The AFM tips are made of silicon, designed to be optimal for measuring topography of soft samples (Oxford Instruments, Santa Barbara, CA). These have a resonant frequency of 70 kHz and force constant of 2 N/m. The AFM images are taken in contact mode with the IGOR Pro 6.37 software (WaveMetrics, Portland, OR). The software used for topography visualization and quantification is Gwyddion, a scanning probe microscopy data analysis application (Department of Nanometrology, Czech Metrology Institute, Czech Republic). Wrinkle amplitude is obtained by finding the RMS (root mean square) roughness (Sq) within the program's statistical analysis tool; wrinkle wavelength is calculated by finding the average wavelength of wrinkles within each AFM scan. Twelve samples were taken of each set of wrinkle formation parameters, from three separate membranes.

Wrinkled Membrane Preparation for Cell Culture

The wrinkled membranes themselves are not suitable for cell culture – they must first be modified, to be able to contain cell culture media while staying sterile. The membranes are first soaked in 100% ethanol for at least 24 hours to remove un-crosslinked oligomers lingering in the PDMS. Even cured properly, solid PDMS has 0-5% of its weight comprised of unlinked polymers (Regehr et al., 2009). Unaccounted for, these can diffuse to the surface of the PDMS even after plasma treatment, blocking hydrophilic surface groups; although PDMS has very low solubility in water, leaching of these chains could be cytotoxic (Regehr et al., 2009). These are then glued using PDMS to custom built cast acrylic frames that will be able to contain the media, and allowed to dry overnight (Figure #). Because cast acrylic cannot be autoclaved and ethanol soak

will dissociate the PDMS from the frame, these are plasma treated for 10 minutes to sterilize the whole assembly while also increasing PDMS hydrophilicity and directly moved to the sterile cell culture hood.

Neonatal Cardiomyocyte Dissection and Culture

Neonatal cardiomyocyte cultures were prepared using 2-day old Sprague-Dawley rats (Charles River Laboratories, Inc., Wilmington, MA). The neonatal hearts were removed and placed into 25 mL Hank's Balanced Salt Solution (HBSS) (Thermo Fisher Scientific, Cambridge, MA) and washed twice in HBSS. After removing the aorta, the hearts are moved to a petri dish and cut into very small pieces within solution and refrigerated at 4°C for 20-24 hours. This was conducted within an animal protocol that is institutionally approved.

The hearts in solution are then transferred into a 50 mL centrifuge tube, and 0.5 mL trypsin inhibitor diluted in HBSS is added and mixed gently. Tissue is oxygenated for 30-60 seconds, and then the tube is placed into a 37°C water bath for 30 seconds. 300 U of collagenase is added to 5 mL Leibovitz's (L-15) media (Thermo Fisher Scientific, Cambridge, MA). This solution is placed on the shaker for 100 minutes, when no solid heart pieces remain. This is then flushed 10 times and filtered through a Falcon 70 um cell strainer (Thermo Fisher Scientific, Cambridge, MA). 5 mL of L-15 media is added to wash remains at bottom, and this is then flushed 10 times gently. This gets filtered through the same film into the same tube and oxygenated for 1 minute before the centrifuge tube with filtered cells goes into the hood at room temperature for 40 minutes.

The solution is centrifuged at 800 rpm for 3 minutes and resuspended gently with DMEM with high glucose and 10% FBS until no more cell clusters at bottom. The cells are plated into two 100 mL cell culture dishes and evenly spread, left in 37°C incubator for 2 hours. The solution is then removed, and dishes flushed 3 times to obtain optimal density of cells. 10 mL media is added to wash out unattached cells. The cell suspension is then counted and aliquoted for use.

Substrate Preparation for Cell Culture

Six hours before cell seeding, the membranes are vacuum-sealed for 15 minutes and plasma treated for 10 minutes to sterilize the membranes and increase hydrophilicity of the naturally hydrophobic PDMS membranes, allowing for adhesion protein attachment (Tan et al., 2010). Although this hydrophilicity increase occurs during wrinkle fabrication, due to the migrations of low molecular weight uncrossed PDMS or residual crosslinking polymers to the surface, the surface returns to its initial hydrophobicity within one to three hours; thus, the plasma treatment is repeated again to increase hydrophilicity (Eddington, Puccinelli, & Beebe, 2006; Vickers, Caulum, & Henry, 2006). The wrinkles are coated with human plasma fibronectin (Merck KGaA, Darmstadt, Germany) diluted at 15 μg/mL i phosphate buffered solution (PBS) a (Corning Life Sciences, Tewksbury, MA). This solution is rinsed with pre-warmed Dulbecco's Modified Eagle Medium (DMEM) (Thermo Fisher Scientific, Cambridge, MA). The cells are seeded at 2.5E+5 cells/cm^2 and supplemental media is added. The DMEM is changed 24 hours after and in 48 hours intervals afterwards.

Cardiomyocyte cultures are then sustained for a 6-day period, fixed in 4% paraformaldehyde (PFA) (Sigma Aldrich, Natick, MA), then stored in 1x phosphate-buffered saline (PBS) (Corning Life Sciences, Tewksbury, MA) until read to be stained.

Cardiomyocyte Characterization

α-Actinin Immunostaining

The fixed cardiomyocytes, kept in PBS in the fridge until used, are stained for α-actinin to observe alignment of cells on the wrinkles. The cells are treated with 0.025% Triton X-100 (Sigma Aldrich, Natick, MA) to allow antibodies to permeate the cell membranes. The samples are then blocked with 10% Normal Donkey Serum (NDS) (Sigma Aldrich, Natick, MA) to prevent unspecific binding of antibodies. The 1st antibody Monoclonal Anti-α-actinin mouse (Sigma Aldrich, Natick, MA) diluted 1:400 is added for 12-24 hours in the fridge; followed washing with 1x PBS thrice at 5 minutes each, the 2nd antibody Donkey anti-Mouse igG, Alexa Fluor 594 (Thermo Fisher Scientific, Cambridge, MA) is then diluted 1:200 and added and allowed to sit for 12-24 hours in the fridge and in complete darkness. This is then washed with 1x PBS thrice at 15 minutes each again to rinse off excess unbound antibodies.

α-Actinin Imaging

Samples treated with antibodies are mounted onto glass coverslips (Corning Incorporated, Corning, NY) with ProLong Gold Antifade Mountant with DAPI (Thermo Fisher Scientific, Cambridge, MA). Cardiomyocytes were viewed using an EVOS Imaging System (Thermo Fisher Scientific, Cambridge, MA) with Plan-APOCHROMAT

63x Oil Immersion Objective (Carl Zeiss Microscopy GmbH, Jena, Germany) and Immersol 518F Immersion Oil (Carl Zeiss Microscopy GmbH, Jena, Germany); images taken using EVOS Imaging System as well. The image files were converted to a .tiff format and the length. The .tiff images are uploaded on a Matlab program established by the research group that uses Fast Fourier Transform (FFT) to find the alignment.

Statistical Analysis

Minitab 19 software was used for statistical analysis**.** Two-way ANOVA is performed in conjunction with Tukey's Honest Significance Test (HST) to compare multiple group. The groups are considered significantly different if $p < 0.05$.

Results

Wrinkled Membrane Characterization

With three strain release rates and three plasma treatment times all at 50% strain, there are nine different samples of wrinkle formation parameters, each with n=12 AFM scans. The results in Graph 2.1 show the averages of these when looking at influence of plasma treatment time keeping strain release rate constant. The results in Graph 2.2 show the averages when looking at influence of strain release constant while keeping plasma treatment time constant.

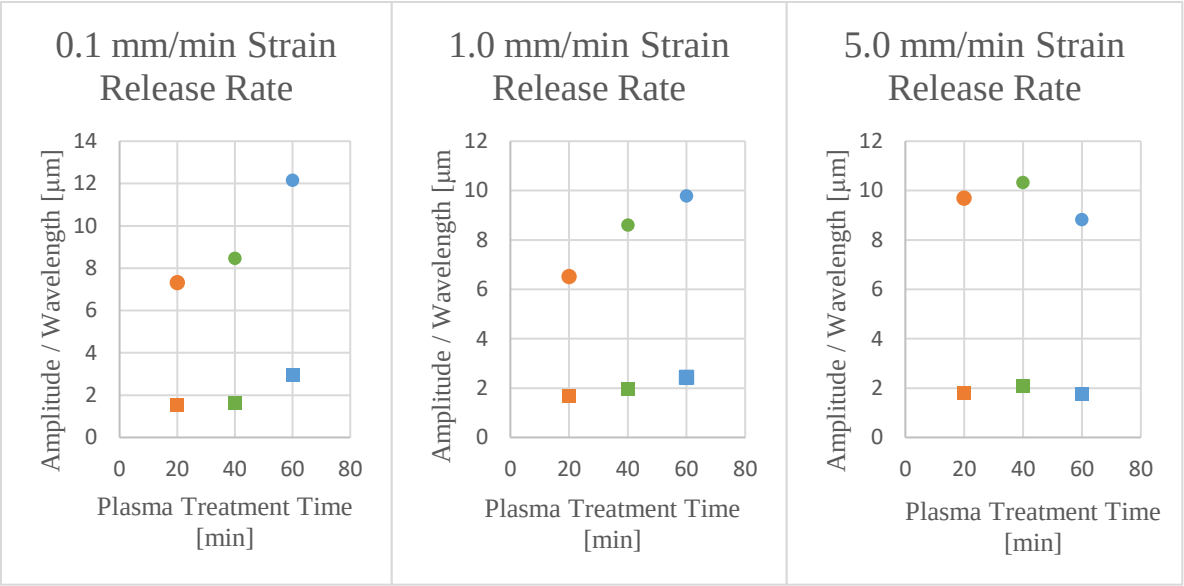

Graph 2.1: Amplitudes and wavelengths of wrinkles based on changing plasma treatment time. Circles represent amplitudes and squares represent wavelengths. Respective pairs are of the same color.

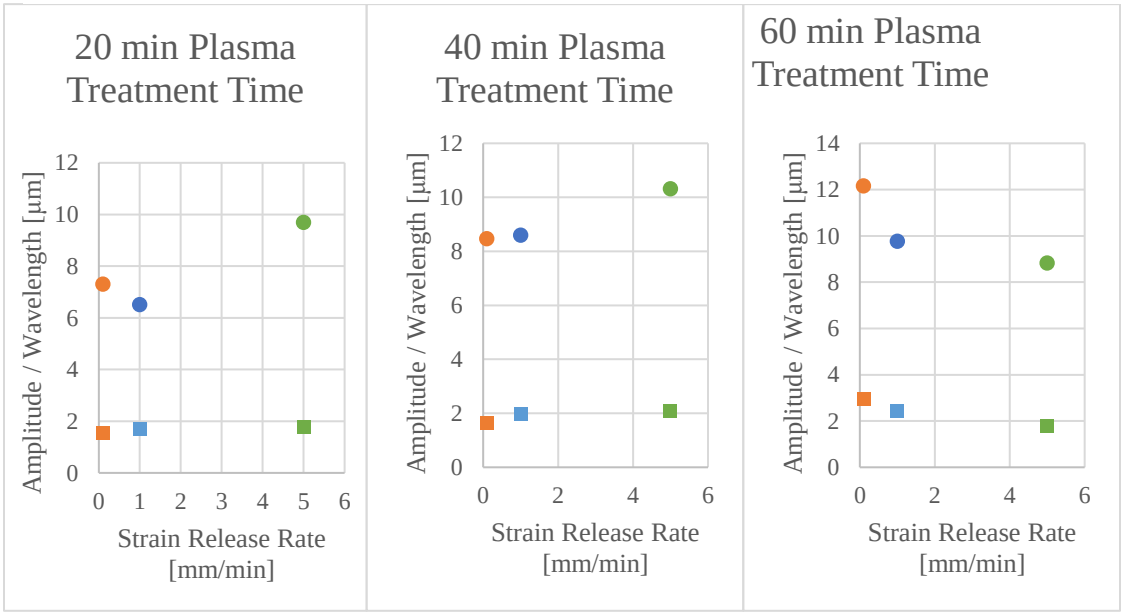

Graph 2.2: Amplitudes and wavelengths of wrinkles based on changing strain release time. Circles represent amplitudes and squares represent wavelengths. Respective pairs are of the same color.

Graph 2.3 illustrates the overall scatter plot of wavelengths and amplitudes based on the wrinkle formation parameters.

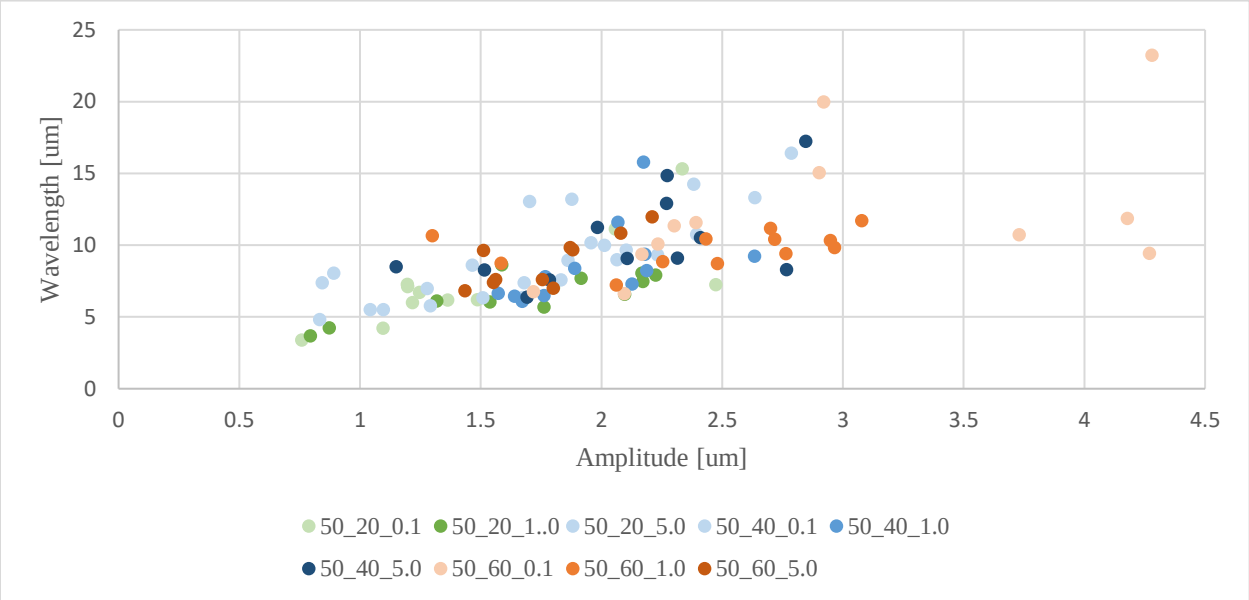

Graph 2.3: Scatter plot of all wavelengths and amplitudes of all wrinkle formation parameters

Two-way ANOVA was used to analyze whether strain release rate or plasma treatment time made a statistically significant difference in the topography. The wrinkle amplitudes and wavelengths were both found to have a P-value of less than 0.05 (0.000000136 and 0.003394, respectively) for plasma treatment time, while strain release rate did not have statistically significant differences (P= 0.444, P= 0.145, respectively).

Source of Variation	F	P-Value	F critical
Sample	0.819	0.444	3.088
Columns	4.745	1.36 E -06	3.088
Interaction	2.367	1.79 E -05	2.464

Table 2.1: Results for 2-way ANOVA for wrinkle amplitudes

Source of Variation	F	P-Value	F critical
Sample	1.968	0.145	3.088
Columns	6.025	0.004	3.088
Interaction	3.670	0.008	2.464

Table 2.1: Results for 2-way ANOVA for wrinkle wavelengths

Tukey's honest significant difference (HSD) test was used to examine if the means are significantly different from each other using Minitab 19. The wavelength and amplitude were both not found to have any difference of means in relation to strain release rate. For plasma treatment time, 20 and 60 minutes were found to be statistically significant in respect to wavelength, but neither with 40 minutes of plasma. For amplitude, plasma treatment time of 60 minutes was found to have a difference of means compared to 40 and 20 minutes, but neither to each other.

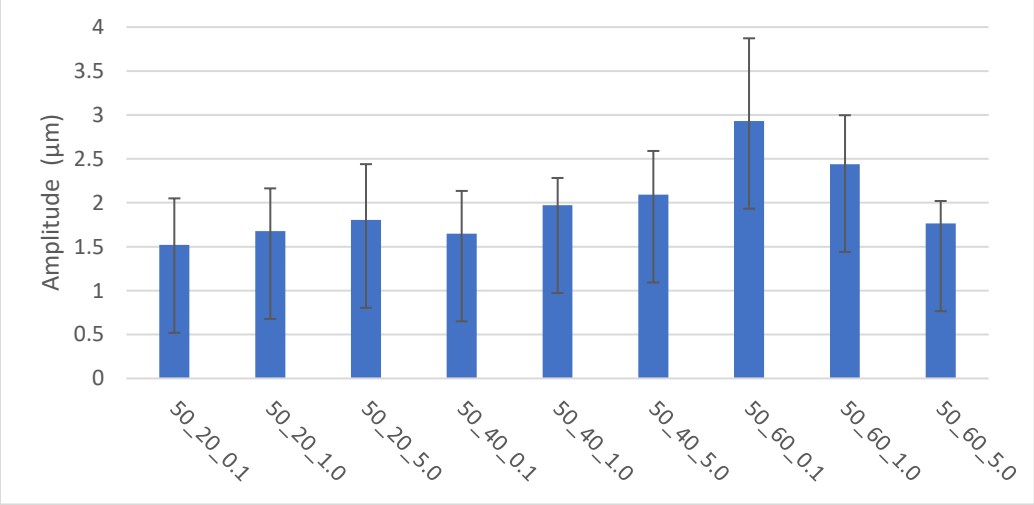

Graph 2.4: Average amplitude of different wrinkled PDMS. Error bars are standard deviation.

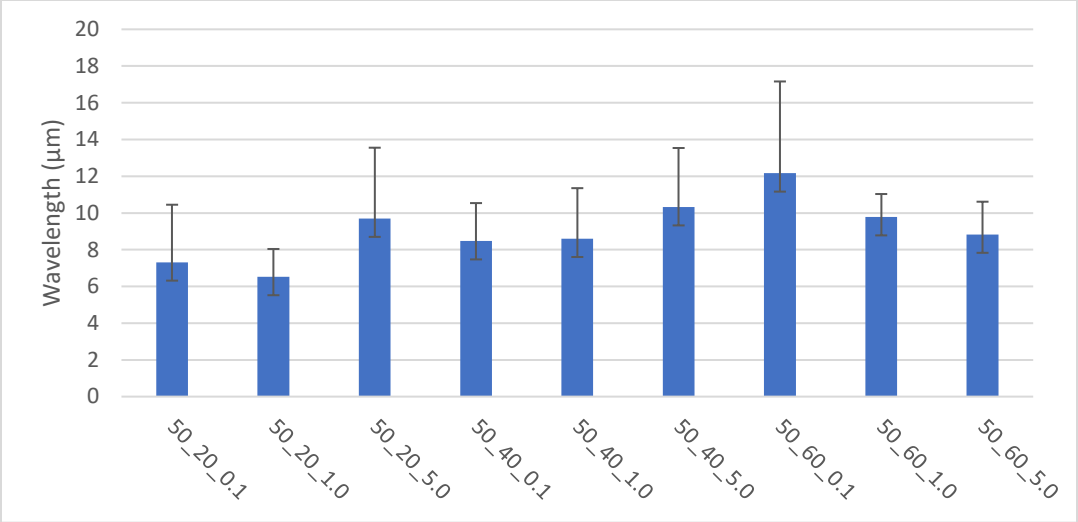

Graph 2.5: Average wavelength of different wrinkled PDMS. Error bars are standard deviation

Cardiomyocyte Alignment

To observe the morphological maturity of the cultured neonatal cardiomyocytes, the cells were stained for α-actinin. The cells were stained with procedures stated above and images taken on the EVOS System with applicable filters. This was analyzed using a customized MATLAB program.

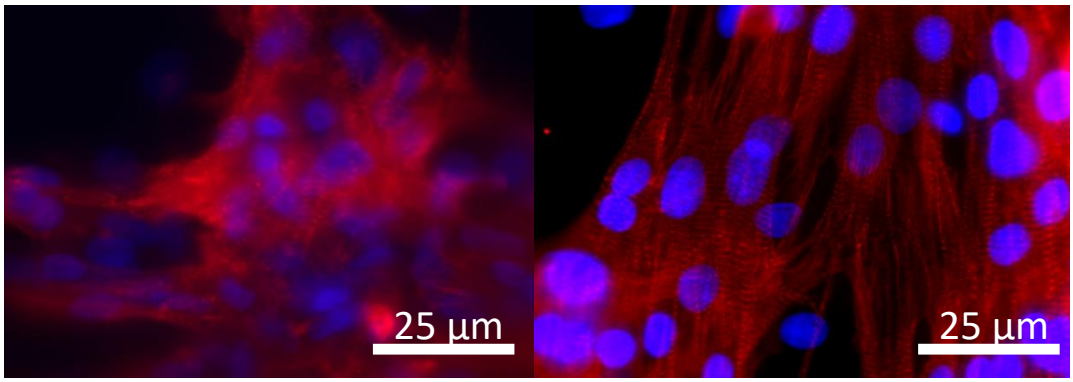

Figure 2.7: α-actinin and DAPI stains of 7-day old cultured rat neonatal cardiomyocytes. Left: flat PDMS Right: Wrinkled PDMS

Wrinkle Formation Parameters	Average Alignment	Samples Analyzed
50_20_0.1	0.763±0.079	53
50_20_1.0	0.776±0.053	121
50_20_5.0	0.885±0.034	11
50_40_0.1	0.755±0.091	86
50_40_1.0	0.690±0.094	54
50_40_5.0	0.869±0.037	14
50_60_0.1	0.811±0.055	32
50_60_1.0	0.783±0.081	27
50_60_5.0	0.768±0.173	29
Control	0.586±0.034	18

Table 2.2: Average alignment values for the different wrinkle parameters

As seen in Figure 2.7, the cardiomyocytes fluoresced red in clear aligned striations when developed morphologically. With the unaligned cells on the left in Figure 2.7 some striations are seen but not aligned well.

Using Tukey's HSD test once again to test for difference in means, the control flat PDMS had significantly different mean from any of the wrinkles; none of the wrinkles were significantly different from each other regardless of the plasma treatment time or strain release rate.

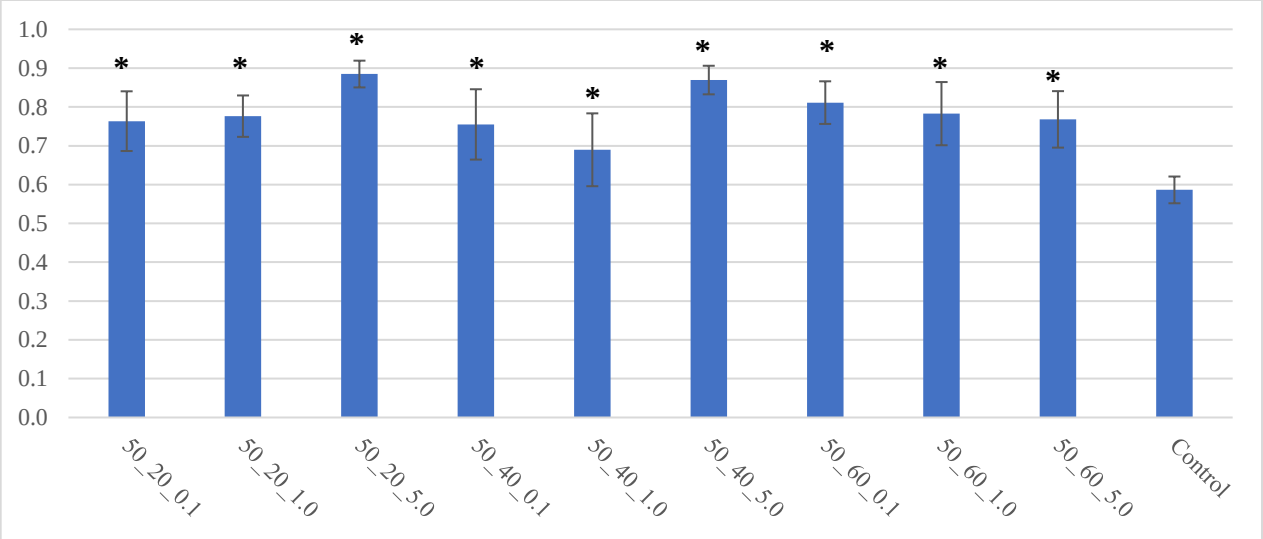

Graph 2.6: Alignment values for different wrinkle parameters against the control (flat). Asterisks indicate statistical different from control ($p<0.05$). No other samples were significantly different from each other.

Discussion

Scale of Wrinkles

Despite indications of plasma treatment leading only to wrinkles in the sub-micrometer scale, we have successfully created wrinkles within the micro range using this method (Rodríguez-Hernández, 2015).

Nano-Level Wrinkles

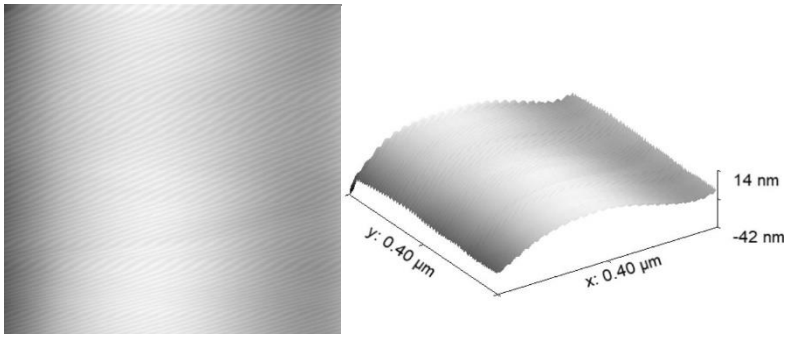

Figure 2.8: Nano-level wrinkles on 50_20_1.0 wrinkles as visualized by AFM

The RMS roughness of these nano-wrinkles was calculated to be 7.96 nm, and the wavelengths of these approximately 1.09 nm. Note that these are not exactly in line with the larger micron-level wrinkles, slightly off angle. This is due to effects of the Poisson's ratio. Elastic materials such as PDMS have a higher Poisson's ratio, which is the strain difference between different juxtapose materials (Lee, Chung, Song, Kim, & Hong, 2013). In our case, this is the stiffer surface of the PDMS and the softer bulk beneath. We can reason that this imitates the heterogeneous nature of ECM in vivo, since organic features are not geometrically perfect. This would also be on the scale of fibers that exist in ECM, since they have been measured to be in the nanometer range, as well as the micrometer range. Thus, our wrinkles are able to imitate that imperfect contour to be able to align the cell geometry.

Discrepancies in Wrinkle Profile

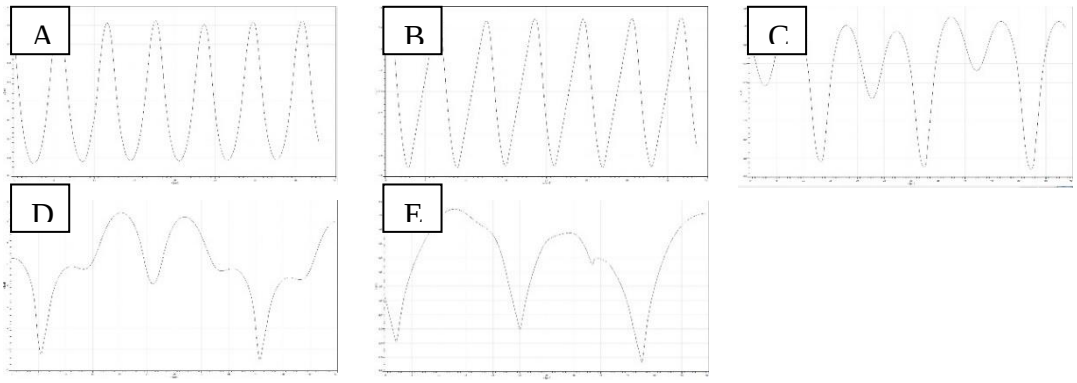

Figure 2.9: Different AFM profiles observed in formulated wrinkles. A. Sinusoidal B. Triangular C. Overlapping Double Bump D. Overlapping Irregular Double Bumps E. Single Bumps

The wrinkle profile varied at a highly random rate, with no correlation to formation parameters observed except that irregularities are more likely to occur at higher plasma treatment times. The different types of wrinkles found via AFM were sinusoidal,

singular bump, overlapping double bumps, and overlapping irregular double bumps, as shown in Figure 15. Both the single and double bumps are likely caused by sinusoidal profiles colliding with each other and overlapping, to different extents.

Defects and Cracks

In the formation of wrinkles, defects and cracks can occur. A defect is defined as where the wrinkle waves overlap, and cracks are imperfections parallel to the wave orientation, caused by the top layer's stiffness (Rodríguez-Hernández, 2015). Studies have shown that cracks diminish with faster release of strain, but the occurrence of defects decreases with a slower release rate (Rodríguez-Hernández, 2015; Schweikart & Fery, 2009). This is due to the effects of the Poisson ratio. Perpendicular fractures happen when the Poisson's stress is higher than the stiff film's critical stress of failure (Chen & Crosby, 2014).

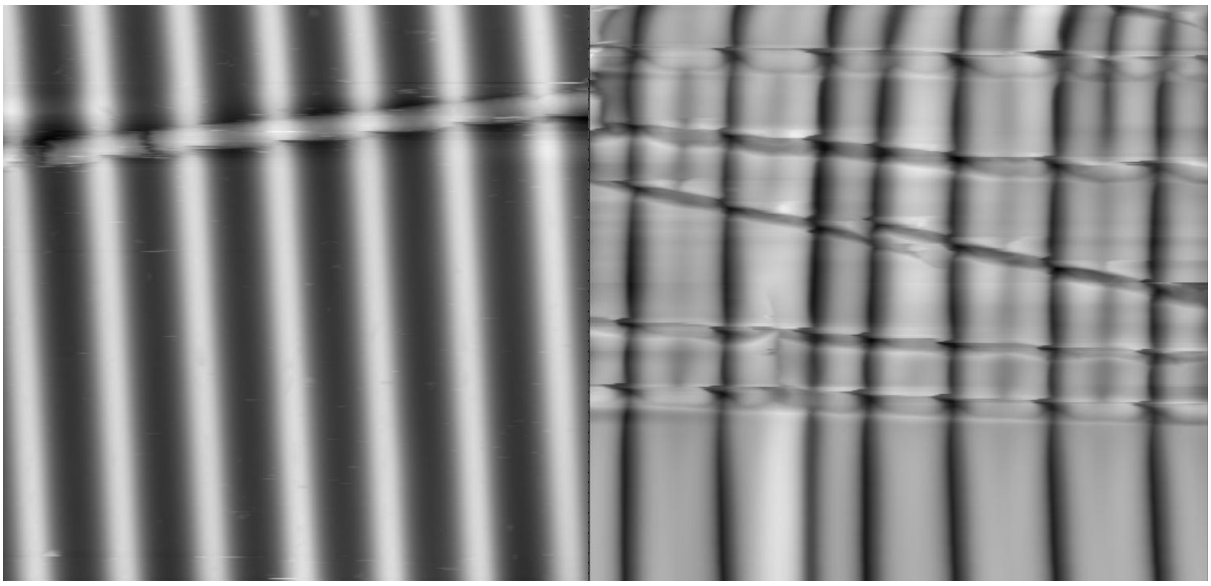

Figure 2.10: Singular and multiple cracks

Plasma Treatment

Since the efficiency of surface oxidation is dependent on the gas(es) present within the chamber, using air plasma is likely to have had an influence on the wrinkles (Nania et al., 2015). Although the amount of oxygen within air is at about 21%, using a pure gas such as O_2 or CO_2 would have allowed for more precision and certainty with the process.

Wrinkle Parameters

Grooves that are too wide and deep allow for cell elongation and alignment to some extent, but when the cells are constrained to be too far apart they cannot communicate to engage in electromechanical coupling (Au et al., 2009). Depth of grooves are more important than width for alignment, since the depth dictates the extent of focal adhesion confinement, thus influencing cytoskeleton alignment (Au et al., 2009). Khine et al. developed a method of creating wrinkles on polyethylene via oxygen plasma treatment, similar to our approach. They found that though their wrinkles have variable topography, it was able to align hESC-CMs well because it matched the features of *in vivo* ECM more accurately such as collagen fiber thickness, texture, and arrangement (US 9.452,564 B2, 2016).

Zhu et al. found that their neonatal cardiomyocytes best aligned at equal to or less than 2 μm, since deeper channels caused cell communication to be weaker due to increased odds of isolation (Zhu et al., 2018). Since the wrinkles we fabricated are all within the 1.5-2.0 μm depth range, this is in agreement with their conclusion, since we are able to successfully culture cells with improved alignment.

Wavelengths and Amplitudes

No statistical difference was found for changing the strain release rate for either wrinkles or amplitudes, but both were found to be influenced by plasma treatment time. This aligns with the results from Khine et al., who found that their oxygen-plasma wrinkled polyethylene's topography was dominantly influenced by exposure time to plasma (US 9.452,564 B2, 2016).

PDMS Hydrophobicity

Although established extraction methods exist for removing unlinked polymers within the PDMS, they have not been shown to significantly affect the hydrophobicity long term; rather, cured PDMS stored in water in particular but also either ethanol or PBS have strongly improved ability to retain hydrophilicity following plasma treatment compared to storage in air, maintaining a water contact angle of less than 90° (B. Kim, Peterson, & Papautsky, 2004).

Cell Culture

Uncured PDMS oligomers may potentially have affected the cell culture. Although ethanol was used to extract uncrossed PDMS oligomers, there is a possibility that this did not fully remove these polymer chains, which may have interacted with the cell culture negatively. Because of the hydrophobic nature of the lipid bilayer's inner membrane, the PDMS oligomers could come in contact with the cardiomyocyte membranes and accumulate, altering cell behavior (Regehr et al., 2009).

Free PDMS oligomers has been found to restrict myosin motility in vitro, only reversed by rigorous chemical extraction or aging for over twenty days (Y. Wang & Burghardt, 2018). The PDMS membranes were soaked in 100% ethanol for at least 48 hours before being in contact with cells for Aim 1; however, going forward seeing the apparent negative influence of free PDMS oligomers in cell culture, they will be soaked for a longer period of time in both ethanol and deionized water for Aim 2 studies.

Cardiomyocyte Alignment

Sarcomeric α-actinin links actin filaments to Z-lines, crosslinking thin filaments in juxtapose sarcomeres, and is present in both neonatal and adult cells (Au et al., 2009). This was stained for to observe cellular organization, as it is found along with other contractile proteins to be continually more organized as the heart develops *in vivo*.

Topographical cues restrict cell adhesion molecules, such as focal adhesions, to the ridges, orienting them parallel the cues; ECM proteins will then orient parallel to the topography as well, affecting the orientation of integrins, which are further associated with the actin cytoskeleton to orient actin parallel to the topography as well (Au et al., 2009). Thus, topography is highly influential on overall cell alignment in a cascading manner.

Although all the wrinkles resulted in improved alignment compared to the control, 50_20_1.0 is chosen for studying electrophysiology in Aim 2 because of the higher sample size and lower standard deviation associated with its satisfactory alignment

coefficient of 0.776. Although other wrinkle parameters had higher alignment coefficients, the sample size is smaller and thus less reliable.

Adult vs Neonatal Morphology

Realistically as we aim to imitate *in vivo* adult cell morphology, we still have some shortcomings with neonatal cell morphology. Though we are able to align and elongate the cells more than if they were conventionally grown on a flat surface, the internal physiology is still not identical to fully matured cells in vivo. However, the subcellular morphological development is mostly influenced by the substrate topography. Myofibrillogenesis of neonatal cells not only controls global shaping of overall cell morphology, but plays a very active part in organizing myofibrils within the cardiomyocytes for local alignment of proteins and structures; however, the organization of the cell's rod-like shape is not directly dependent on maturation of microfibrils (Simpson et al., 1994).

Conclusion

In conclusion, wrinkles are able to be fabricated using plasma treatment, though with limited control on the resulting wavelengths and amplitudes. Plasma treatment time had a clear statistical influence on the wrinkle parameters, while strain release rate did not, opposing some existing studies. Despite variation in the topography, all wrinkles resulted in improved cardiomyocyte aligning compared to flat PDMS.

All wrinkles showed statistically significant improvement of alignment compared to flat PDMS, but the results of these were not significantly discernable between each other.

Moving forward to Aim 2, we will be using wrinkles created using 50% stretch, 20 minutes of plasma treatment, and a stretch release rate of 1.0 mm/min (denoted as 50_20_1.0 moving forward). We will compare the calcium cycling abilities of neonatal cardiomyocytes cultured on this wrinkled substrate with established microgrooves fabricated in our research group, as well flat PDMS for a control.

References

Acosta-torres, Z., Bax, N. A. M., Spreeuwel, A. C. C. Van, & Bouten, C. V. C. (2013). Developing engineered cardiac tissue models from HL-1 cardiomyocytes and mouse embryonic fibroblasts. In *29th Southern Biomedical Engineering Conference* (pp. 39–40). https://doi.org/10.1109/SBEC.2013.28

Au, H. T. H., Cui, B., Chu, Z. E., Veres, T., & Radisic, M. (2009). Cell culture chips for simultaneous application of topographical and electrical cues enhance phenotype of cardiomyocytes. *Lab on a Chip*, *9*(4), 564–575. https://doi.org/10.1039/b810034a

Bae, W., Kim, J., Choung, Y., Chung, Y., Suh, K. Y., Pang, C., … Eui, H. (2015). Bio-inspired configurable multiscale extracellular matrix-like structures for functional alignment and guided orientation of cells. *Biomaterials*, *69*, 158–164. https://doi.org/10.1016/j.biomaterials.2015.08.006

Besser, R. R., Ishahak, M., Mayo, V., Carbonero, D., Claure, I., & Agarwal, A. (2018). Engineered microenvironments for maturation of stem cell derived cardiac myocytes. *Theranostics*, *8*(1), 124–140. https://doi.org/10.7150/thno.19441

Bhattacharya, S., Datta, A., Berg, J. M., & Gangopadhyay, S. (2014). Studies on Surface Wettability of Studies on Surface Wettability of Poly (Dimethyl) Siloxane (PDMS) and Glass Under Oxygen-Plasma Treatment and Correlation With Bond Strength, *14*(June), 590–597. https://doi.org/10.1109/JMEMS.2005.844746

Bowden, N., Huck, W. T. S., Paul, K. E., & Whitesides, G. M. (1999). The controlled formation of ordered , sinusoidal structures by plasma oxidation of an elastomeric polymer. *Applied Physics Letters*, *75*(17), 2557–2559. https://doi.org/10.1063/1.125076

Campo, A. (2015). Fabrication of hierarchical wrinkled morphologies through sequential UVO treatments. *Journal of Applied Polymer Science*, *41863*, 1–9. https://doi.org/10.1002/app.41863

Cao, C., Chan, H. F., Zang, J., Leong, K. W., & Zhao, X. (2014). Harnessing Localized Ridges for High-Aspect-Ratio Hierarchical Patterns with Dynamic Tunability and Multifunctionality Changyong. *Advanced Materials*, *26*(11), 1763–1770. https://doi.org/10.1002/adma.201304589.Harnessing

Carson, D., Hnilova, M., Yan, X., et al. (2016). Nanotopography-Induced Structural Anisotropy and Sarcomere Development in Human Cardiomyocytes Derived from Induced Pluripotent Stem Cells. *ACS Appl Mater Interfaces*, *8*(34), 21923–21932. https://doi.org/10.5588/ijtld.16.0716.Isoniazid

Carson, D., Hnilova, M., Yang, X., Nemeth, C. L., Tsui, J. H., Smith, A. S. T., … Kim, D. H. (2016). Nanotopography-Induced Structural Anisotropy and Sarcomere Development in Human Cardiomyocytes Derived from Induced Pluripotent Stem Cells. *ACS Applied Materials and Interfaces*. https://doi.org/10.1021/acsami.5b11671

Chen, Y. C., & Crosby, A. J. (2014). High aspect ratio wrinkles via substrate prestretch. *Advanced Materials*, *26*(32), 5626–5631. https://doi.org/10.1002/adma.201401444

Chlopčíková, Š., Psotová, J., & Miketová, P. (2001). Neonatal Rat Cardiomyocytes - A Model for the Study of Morphological, Biochemical, and Electrophysiological Characteristics of the Heart (Chlopcikova), *145*(2), 49–55.

Eddington, D. T., Puccinelli, J. P., & Beebe, D. J. (2006). Thermal aging and reduced hydrophobic recovery of polydimethylsiloxane. *Sensors and Actuators, B: Chemical*, *114*(1), 170–172. https://doi.org/10.1016/j.snb.2005.04.037

Efimenko, K., Rackaitis, M., Manias, E., Vaziri, A., Mahadevan, L., & Genzer, J. A. N. (2005). Nested self-similar wrinkling patterns in skins. *Nature Materials*, *4*(April), 293–297. https://doi.org/10.1038/nmat1342

Efimenko, K., Wallace, W. E., & Genzer, J. (2002). Surface modification of Sylgard-184 poly(dimethyl siloxane) networks by ultraviolet and ultraviolet/ozone treatment. *Journal of Colloid and Interface Science*, *254*(2), 306–315. https://doi.org/10.1006/jcis.2002.8594

George, A. C. O. (2014). *Scalable Topography-Induced Cell Alignment for Tissue Engineering Applications*. National University of Singapore.

Hu, J., Hardy, C., Chen, C. M., Yang, S., Voloshin, A. S., & Liu, Y. (2014). Enhanced cell adhesion and alignment on micro-wavy patterned surfaces. *PLoS ONE*, *9*(8), 2–9. https://doi.org/10.1371/journal.pone.0104502

Jiang, X., Takayama, S., Qian, X., Ostuni, E., Wu, H., Bowden, N., … Whitesides, G. M. (2002). Controlling Mammalian Cell Spreading and Cytoskeletal Arrangement with Conveniently Fabricated Continuous Wavy Features on Poly (dimethylsiloxane). *Langmuir*, *18*, 3273–3280.

Juan Rodriguez-Hernandez, A. C. (2015). Fabrication of hierarchical wrinkled morphologies through sequential UVO treatments. *Journal of Applied Polymer Science*, *41863*, 1–9. https://doi.org/10.1002/app.41863

Khine, M., Li, R. A., & Chen, C.-W. (2016). *US 9.452,564 B2*. United States. https://doi.org/US005485919A

Kim, B., Peterson, E. T. K., & Papautsky, I. (2004). Long-Term Stability of Plasma Oxidized PDMS Surfaces. *Proceedings of the 26th Annual International Conference of the IEEE EMBS*, 5013–5016.

Kim, D. H., Lipke, E. A., Kim, P., Cheong, R., Thompson, S., Delannoy, M., … Levchenko, A. (2010). Nanoscale cues regulate the structure and function of macroscopic cardiac tissue constructs. *Proceedings of the National Academy of Sciences*, *107*(2), 565–570. https://doi.org/10.1073/pnas.0906504107

Kleber, A. G., & Rudy, Y. (2004). Basic Mechanisms of Cardiac Impulse Propagation and Associated Arrhythmias. *Physiol Rev*, *84*, 431–488.

Lee, J., Chung, S., Song, H., Kim, S., & Hong, Y. (2013). Lateral-crack-free, buckled, inkjet-printed silver electrodes on highly pre-stretched elastomeric substrates. *Journal of Physics D: Applied Physics*, *46*(10). https://doi.org/10.1088/0022-3727/46/10/105305

Lin, G., Zhang, Q., Lv, C., Tang, Y., & Yin, J. (2018). Small degree of anisotropic wetting on self-similar hierarchical wrinkled surfaces. *Soft Matter*, *14*(9). https://doi.org/10.1039/C7SM02208E

Luna, J. I., Ciriza, J., Garcia-Ojeda, M. E., Kong, M., Herren, A., Lieu, D. K., … McCloskey, K. E. (2011). Multiscale Biomimetic Topography for the Alignment of Neonatal and Embryonic Stem Cell-Derived Heart Cells. *Tissue Engineering Part C: Methods*, *17*(5), 579–588. https://doi.org/10.1089/ten.tec.2010.0410

Macfarlane, P., van Oosterom, A., Pahlm, O., Kligfield, P., Janse, M., & Camm, J. (2010). *Comprehensive Electrocardiology*. *Comprehensive Electrocardiology* (Vol. 1). https://doi.org/10.1007/978-1-84882-046-3

Mandenius, C. F., Steel, D., Noor, F., Meyer, T., Heinzle, E., Asp, J., … Sartipy, P. (2011). Cardiotoxicity testing using pluripotent stem cell-derived human cardiomyocytes and state-of-the-art bioanalytics: A review. *Journal of Applied Toxicology*, *31*(3), 191–205. https://doi.org/10.1002/jat.1663

Manring, H. R., Dorn, L. E., Ex-willey, A., Accornero, F., & Ackermann, M. A. (2018). At the heart of inter- and intracellular signaling : the intercalated disc. *Biophysical Reviews*, *10*, 961–971.

Martínez, E., Engel, E., Planell, J. A., & Samitier, J. (2009). Effects of artificial micro- and nano-structured surfaces on cell behaviour. *Annals of Anatomy*, *191*(1), 126–135. https://doi.org/10.1016/j.aanat.2008.05.006

Mathur, A., Ma, Z., Loskill, P., Jeeawoody, S., & Healy, K. E. (2016). In vitro cardiac tissue models: Current status and future prospects. *Advanced Drug Delivery Reviews*, *96*, 203–213. https://doi.org/10.1016/j.addr.2015.09.011

McCain, M. L., & Parker, K. K. (2011). Mechanotransduction: The role of mechanical stress, myocyte shape, and cytoskeletal architecture on cardiac function. *European Journal of Physiology*, *462*, 89–104. https://doi.org/10.1007/s00424-011-0951-4

McDevitt, T. C., Angello, J. C., Whitney, M. L., Reinecke, H., Hauschka, S. D., Murry, C. E., & Stayton, P. S. (2002). In vitro generation of differentiated cardiac myofibers on micropatterned laminin surfaces. *J Biomed Mater Res*, *60*, 472–479. https://doi.org/10.1008/jbm.1292

Mei, Y., Kiravittaya, S., Harazim, S., & Schmidt, O. G. (2010). Principles and applications of micro and nanoscale wrinkles. *Materials Science and Engineering R: Reports*, *70*(3–6), 209–224. https://doi.org/10.1016/j.mser.2010.06.009

Moon, M. W., & Vaziri, A. (2009). Surface modification of polymers using a multi-step plasma treatment. *Scripta Materialia*, *60*(1), 44–47. https://doi.org/10.1016/j.scriptamat.2008.08.038

Nania, M., Matar, O. K., & Cabral, J. T. (2015). Frontal vitrification of PDMS using air plasma and consequences for surface wrinkling. *Soft Matter*, *11*(15), 3067–3075. https://doi.org/10.1039/c4sm02840f

Noorman, M., Heyden, M. A. G. Van Der, Veen, T. A. B. Van, Cox, M. G. P. J., Hauer, R. N. W., Bakker, J. M. T. De, & Rijen, H. V. M. Van. (2009). Cardiac cell – cell junctions in health and disease : Electrical versus mechanical coupling. *Journal of Molecular and Cellular Cardiology*, *47*(1), 23–31. https://doi.org/10.1016/j.yjmcc.2009.03.016

Regehr, K. J., Domenech, M., Koepsel, J. T., Carver, K. C., Ellison-zelski, J., Murphy, W. L., … David, J. (2009). Biological implications of polydimethylsiloxane-based microfluidic cell culture. *Lab on a Chip*, *9*(15), 2132–2139. https://doi.org/10.1039/b903043c.Biological

Rodríguez-Hernández, J. (2015). Wrinkled interfaces: Taking advantage of surface instabilities to pattern polymer surfaces. *Progress in Polymer Science*, *42*, 1–41. https://doi.org/10.1016/j.progpolymsci.2014.07.008

Saini, H., Sam, F. S., Kharaziha, M., & Nikkhah, M. (2015). Micropatterning Techniques to Control Cell-Biomaterial Interface for Cardiac Tissue Engineering. In *Cell and Material Interface: Advances in Tissue Engineer, Biosensor, Implant, and Imaging Technologies* (pp. 187–214).

Schweikart, A., & Fery, A. (2009). Controlled wrinkling as a novel method for the fabrication of patterned surfaces. *Microchim Acta*, *165*, 249–263. https://doi.org/10.1007/s00604-009-0153-3

Sheikh, F., Ross, R.S., and Chen, J. (2009). Cell-Cell Connection to Cardiac Disease. *Trends Cardiovasc Meds*, *19*(6), 182–190. https://doi.org/10.3174/ajnr.A1256.Functional

Sigg, D. C. ., Laizzo, P. A. ., Xiao, Y.-F., & He, B. (2010). *Cardiac Electrophysiology Methods and Models*. *Cardiac Electrophysiology Methods and Models*. https://doi.org/10.1007/978-1-4419-6658-2

Simmons, C. S., Petzold, B. C., & Pruitt, B. L. (2012). Microsystems for biomimetic stimulation of cardiac cells. *Lab on a Chip*, *12*(18), 3235–3248. https://doi.org/10.1039/c2lc40308k

Simpson, D. G., Terracio, L., Terracio, M., Price, R. L., Turner, D. C., & Borg, T. K. (1994). Modulation of Cardiac Myocyte Phenotype In Vitro by the Composition and Orientation of the Extracellular Matrix. *Journal of Cellular Physiology*, *161*, 89–105.

Soares, C. P., Midlej, V., de Oliveira, M. E. W., Benchimol, M., Costa, M. L., & Mermelstein, C. (2012). 2D and 3D-organized cardiac cells shows differences in cellular morphology, adhesion junctions, presence of myofibrils and protein expression. *PLoS ONE*, *7*(5). https://doi.org/10.1371/journal.pone.0038147

Später, D., Hansson, E. M., Zangi, L., & Chien, K. R. (2014). How to make a cardiomyocyte. *Development (Cambridge)*, *141*(23), 4418–4431. https://doi.org/10.1242/dev.091538

Swaminathan, S., Bullough, M., Li, Q., Zhou, A., & Cui, Y. (2013). Non-lithographic patterning of phage-displayed peptides with wrinkled elastomers. *Journal of the Royal Society Interface*, 1–5.

Tan, S. H., Nguyen, N., & Chua, C. (2010). Oxygen plasma treatment for reducing hydrophobicity of a sealed polydimethylsiloxane microchannel. *Biomicrofluidics*, *4*, 1–8. https://doi.org/10.1063/1.3466882

Veeraraghavan, R., Gourdie, R. G., & Poelzing, S. (2014). Mechanisms of cardiac conduction : a history of revisions. *Heart Circ Physiol*, *306*, H619–H627. https://doi.org/10.1152/ajpheart.00760.2013

Vickers, J. A., Caulum, M. M., & Henry, C. S. (2006). Generation of hydrophilic poly(dimethylsiloxane) for high-performance microchip electrophoresis. *Analytical Chemistry*, *78*(21), 7446–7452. https://doi.org/10.1021/ac0609632

Voigt, D., Schweikart, A., Fery, A., & Gorb, S. (2012). Leaf beetle attachment on wrinkles : isotropic friction on anisotropic surfaces, (1), 1975–1982. https://doi.org/10.1242/jeb.068320

Wang, P. Y., Yu, H. Te, & Tsai, W. B. (2010). Modulation of alignment and differentiation of skeletal myoblasts by submicron ridges/grooves surface structure. *Biotechnology and Bioengineering*, *106*(2), 285–294. https://doi.org/10.1002/bit.22697

Wang, Y., & Burghardt, T. P. (2018). Uncured PDMS Inhibits Myosin In Vitro Motility in a Microfluidic Flow Cell. *BioRxiv*, 1–23.

Wei, K., & Zhao, Y. (2014). Fabrication of Anisotropic and Herarchical Undulations by Benchtop Surface Wrinkling. *MEMS*, 474–477.

Yap, F. L., & Zhang, Y. (2007). Protein and cell micropatterning and its integration with micro / nanoparticles assembly. *Biosensors and Bioelectronics*, *22*, 775–788. https://doi.org/10.1016/j.bios.2006.03.016

Zheng, H., Liu, S., Tian, W., Yan, H., Zhang, Y., & Li, Y. (2012). A three-dimensional in vitro culture model for primary neonatal rat ventricular myocytes. *Current Applied Physicas*, *12*, 826–833. https://doi.org/10.1016/j.cap.2011.11.014

Zhu, C., Rodda, A. E., Truong, V. X., Shi, Y., Zhou, K., Haynes, J. M., … Forsythe, J. S. (2018). Increased Cardiomyocyte Alignment and Intracellular Calcium Transients Using Micropatterned and Drug-Releasing Poly(Glycerol Sebacate) Elastomers. *ACS Biomaterials Science and Engineering*, *4*(7), 2494–2504. https://doi.org/10.1021/acsbiomaterials.8b00084

Zimmermann, W. H., Fink, C., Kralisch, D., Remmers, U., Weil, J., & Eschenhagen, T. (2000). Three-dimensional engineered heart tissue from neonatal rat cardiac myocytes. *Biotechnology and Bioengineering*, *68*(1), 106–114. https://doi.org/10.1002/(SICI)1097-0290(20000405)6

CHAPTER 3

EXAMINING THE CALCIUM CYCLING BETWEEN CARDIOMYOCYTES UNDER DIFFERENT CELL MORPHOLOGIES

Introduction

Given the successful morphological development of cardiomyocyte cultures, we wanted to explore the successful electrical integration of these cells. To prove this, there must be indication of electrical signal propagation, thus the presence of the correct cellular components. If these do not mature fully or have poor distribution, this will reflect in the cell's ability to carry out the excitation-contraction cycle. We will explore calcium cycling, an essential aspect of the cardiomyocyte electrical physiological system, to observe how morphology affects functionality.

Literature Review

Cardiac Level Electrophysiology

The heart's primary function is to pump blood to the rest of the body for transportation of nutrients and waste products. Electrical impulses travel through the heart, allowing it to contract and expel blood properly.

Electrical propagation is initiated in the sinus node and progresses through the atria quickly, making up the P wave in the ECG and is followed by the atria contracting. The impulse then spends about 120 to 200 ms going through the AV node, leading up to the PR interval, where atrial contractions aid the ventricles to fill passively (Macfarlane et

al., 2010). Once past the AV node, the impulse activates the His-Purkinje system, activating the ventricles quickly (represented by the QRS complex, lasting approximately 100 ms) (Macfarlane et al., 2010). The PQRST wave levels out during the ventricular action potential's extended plateau phase, and the T wave occurs when the ventricles finally polarize (Macfarlane et al., 2010).

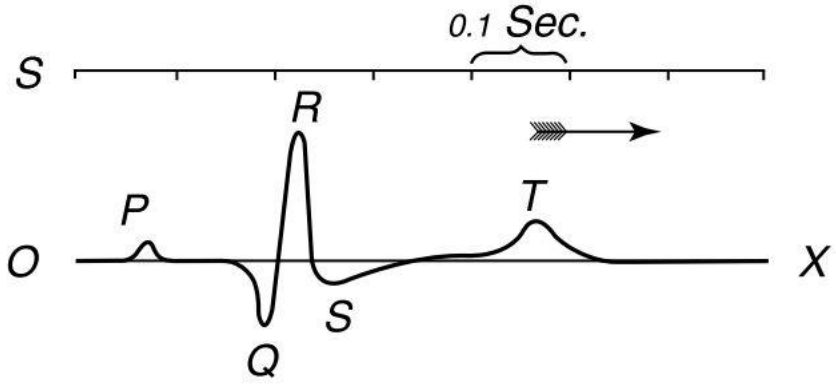

Figure 3.1: PQRST wave of a heartbeat, indicating the transmission of electrical signal through the heart to cause contraction and flow of blood through the body (Reproduced with permission from MacFarlane 2010).

In an adult human heart, it takes about 30 ms for the movement of electrical signal from the sinoatrial and atrioventricular nodes, and 70-90 ms more for atrial triggering. Electrical coupling is essential to global pathophysiology. When conduction velocity is reduced in the myocardium, dilated and hypertrophic cardiomyopathy is more likely, increasing the risk for both sudden cardiac death as well as lethal arrythmias (Manring, Dorn, Ex-willey, Accornero, & Ackermann, 2018).

Cardiomyocyte Level Electrophysiology

On a cellular level, changes in ion concentrations across the cell membrane allow for electrical activity, known as membrane currents. For cardiomyocytes, this typically involves calcium, sodium, potassium, and chloride ions (Sigg, Laizzo, Xiao, & He, 2010). Sodium ions flowing quickly into the cell depolarizes the cell; following this step, calcium ions flow in and potassium ions out to level out the membrane voltage, until continuous movement of potassium ions out of the cell repolarize the membrane back to resting potential (Veeraraghavan, Gourdie, & Poelzing, 2014). Cardiac electrical triggering starts with the depolarization of the cell membrane, initializing the action potential; this is when an external stimulus causes a rapid increase in the voltage differential across the cell membrane (Sigg et al., 2010). Within the ventricle, the conduction velocity in the longitudinal direction of cardiomyocytes is within the range of 0.48-0.61 m/s (Kleber & Rudy, 2004).

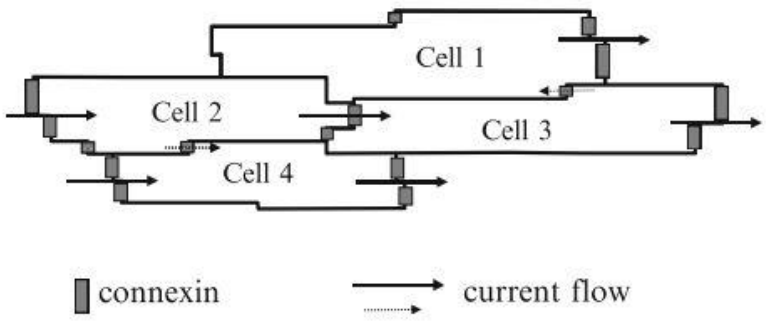

Figure 3.2: Diagram representing the flow of electrical current through cells via longitudinal end interfaces in vivo (Reprinted with permission from Sigg 2010)

Cell Membrane

The cell membrane is comprised of a phospholipid bilayer with channel proteins that allow for selective ion transportation, controlling the ionic concentrations

intracellularly and extracellularly. A cardiomyocyte's resting potential is negative, meaning that the inside of the cell has a more negative charge than the outside by default; when the negativity is reduced, depolarization occurs, triggering the action potential (Sigg et al., 2010).

Each myocyte is surrounded by plasma membrane called sarcolemma, which has many invaginations perpendicular to the long cell axis known as T-tubules, unique to ventricular cardiomyocytes (Macfarlane et al., 2010). These T-tubules, located at increase cell sur sarcomere junctions, face area and have high density of ion channels and transporters to allow for excitation-contraction (EC) coupling (Eisner, Caldwell, Kistamás, & Trafford, 2017; Macfarlane et al., 2010).

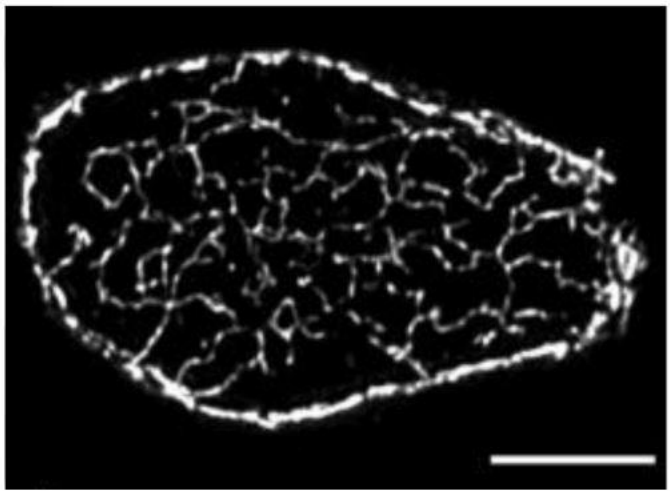

Figure 3.3: Transverse slice of ventricular myocyte showing distribution of T-tubules throughout the cell (Reproduced with permission from Eisner 2017)

The sarcoplasmic reticulum (SR) actively accumulates calcium ions using ATP-driven transport (via SR calcium-ATP-ase, or SERCA) (Macfarlane et al., 2010). The SR is about 10 nm away from the T-tubules on one side and contractile apparatus on the

other, though not actually touching either; this proximity is essential for calcium-induced calcium release (CICR), which is expanded on further below (Macfarlane et al., 2010).

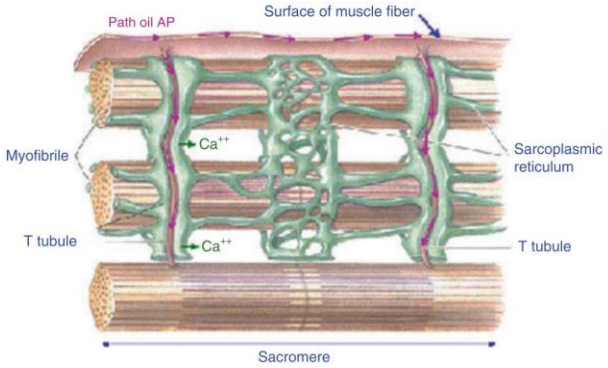

Figure 3.4: Diagram demonstrating distribution of sarcoplasmic reticulum and T tubules in cardiomyocytes in vivo (Reproduced with permission from MacFarlane 2010)

Membrane Electrophysiology

When there is no net movement of ions through the cell membrane, the cardiomyocyte is at resting potential, around -85 to -90 mV typically. The electrical and chemical gradients affect the movement of ions. Voltage-gated ion channels in the cell membrane allow for specific permeability of certain ions; the main types each only let in either calcium, sodium, or potassium (Sigg et al., 2010). Although all of these fluxes and channels play a role in cell functionality, the one of interest to us is the L-type calcium channel, highlighted in Figure 5.

At resting potential, the sodium channels are closed and the potassium ones open; when the sodium channels open, the action potential is initiated. This depolarizes the cell to about +20 mV, causing a calcium ion influx via L-type voltage-gated Ca2+ channel

(VOCCs) activation; this then causes the sarcoplasmic reticulum to release calcium ions intracellularly (Fearnley, Roderick, & Bootman, 2011; Herron, Lee, & Jalife, 2012). This activates the area where actin and sarcomeric myosin filaments interact, causing contraction (Sigg et al., 2010).

I_{Na} causes the sarcoplasmic reticulum (SR) to release calcium via the calcium-induced calcium release (CICR) process, inducing the calcium transient and cell contraction (Kleber & Rudy, 2004). L-type calcium channels slowly close off.

Calcium

Calcium ionic currents are especially important with the excitation-contraction cycle of cardiomyocytes (Zheng et al., 2012). Calcium is primarily moved out of the cytoplasm by either the sarcoendoplasmic reticulum Ca ATPase (SERCA) pathway or the Na/Ca exchanger (NCX) pathway, which make up over 95% of the mechanisms for calcium removal (Hwang et al., 2015).

The detailed movement of calcium ions is essential to the contraction of cardiomyocytes. Within the cell, three components are essential for the generation of Ca^{2+} signals for cellular depolarization as well as recovery of such following contraction: 1) ryanodine receptors (RyR), 2) voltage-gated Ca^{2+} channels (VOCC), and Ca^{2+} pump and transporters (Fearnley et al., 2011; Herron et al., 2012).

These collaborate in units that facilitate calcium release. Each of these units is comprised of 10-25 L-type VOCCs and 100-200 RyRs (Bers, 2008). When calcium flows into the cell via the L-type VOCCs, they move into the space between the plasma

membrane and the SR, known as the dyadic cleft; the ions then accumulate here until the concentration turns from 100 nM to 100 μM, and known as a Ca^{2+} sparklet (Fearnley et al., 2011). However, this alone is not enough calcium for substantial contraction. These Ca^{2+} sparklets induce the opening of ryanodine receptors (RyRs) on the SR; RyR activity affects cytosolic Ca^{2+} concentration (Fearnley et al., 2011; Herron et al., 2012). The calcium concentration in the dyadic cleft after L-type VOCC activation allows for Ca^{2+} - induced Ca^{2+} release (CICR) facilitation – clusters of RyRs activate and mobilize Ca^{2+} from the SR, creating a Ca^{2+} spark, which is the initial Ca^{2+} release signal (Fearnley et al., 2011; Hwang et al., 2015).

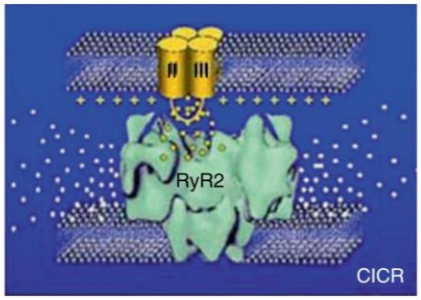

Figure 3.5: Ryanodine receptors on the sarcoplasmic reticulum in CICR (Reprinted with permission from MacFarlane 2010)

The Ca^{2+} concentration in the dyadic cleft then reaches 200 – 400 μM; these ions then diffuse out of the cleft to trigger contraction units, shortening the cell and globally allowing for heart contractions (Bers, 2008; Fearnley et al., 2011; Todd J. Herron, Peter Lee, 2012). Each L-type VOCC on the sarcolemma corresponds to a cluster of RyR channels on the SR, creating a unit for efficient and rapid calcium release (Macfarlane et al., 2010). The involvement of calcium ion transportation is so essential to the function of the heart that Ca^{2+} propagation is often measured simultaneously with the AP to

observe arrhythmias connected to heart failure, and diseased CMs tend to have skewed intercellular calcium cycling that reflects abnormal contraction/relaxation (Herron et al., 2012; Hwang et al., 2015; Prajapati & Po, 2018). RyR distribution has been found to change in vivo following heart failure, with the longitudinal ends having higher density while simultaneously having decreased t-tubule density in this area (Eisner et al., 2017). Inadequate calcium release can cause heart failure (Zhu et al., 2018). Worthwhile to note, the SR actually only releases about half of its calcium stores during the transient (Eisner et al., 2017).

Gap Junctions

In the 1950s, Andersson and Sjőstrand discovered via electron microscopic observation that the myocardium is made up by cells individually wrapped up in cell membranes; because this contradicts previous studies regarding quick electrical propagation in the heart, the scientific community hypothesized that there are low resistance passages through which electrical signals can pass through adjacent cells rapidly (Rohr, 2004). These pathways are called gap junctions and are concentrated at the longitudinal ends, known as intercalated discs, of rod-shaped cardiomyocytes (Rohr, 2004). Although present all around cellular borders in low quantities, they are higher in number and also larger in size at the longitudinal ends (Kleber & Rudy, 2004). These are bundles of channels, anywhere from less than ten to more than tens of thousands, between cells that allow for transfer of small molecules and ions at the lowest resistance pathway; monomers called connexons form groups of six to create connexins, the basic unit of gap junctions (Manring et al., 2018; Severs, Bruce, Dupont, & Rothery, 2008).

Two juxtapose connexons of adjacent cells create the bridge to allow for small molecule and electrical signal movement (Kleber & Saffitz, 2014; Macfarlane et al., 2010). In humans, there are 21 different types of connexons that bind together in various combinations to form intercellular channels of various physiological abilities (Goodenough & Paul, 2009). In vitro studies of uncoupling the cells by decreasing gap junction conductance leads to slower propagation, and in some cases change the direction of intended signal flow (Kleber & Saffitz, 2014). Distribution of gap junctions is also important to note – when acute cardiac infarction occurs, ventricular cardiomyocytes surrounding the scar tissue undergo remodeling of Cx43, redistributing them to the lateral borders of the cell; this is pro-arrhythmic and alters conduction velocity (Severs et al., 2008).

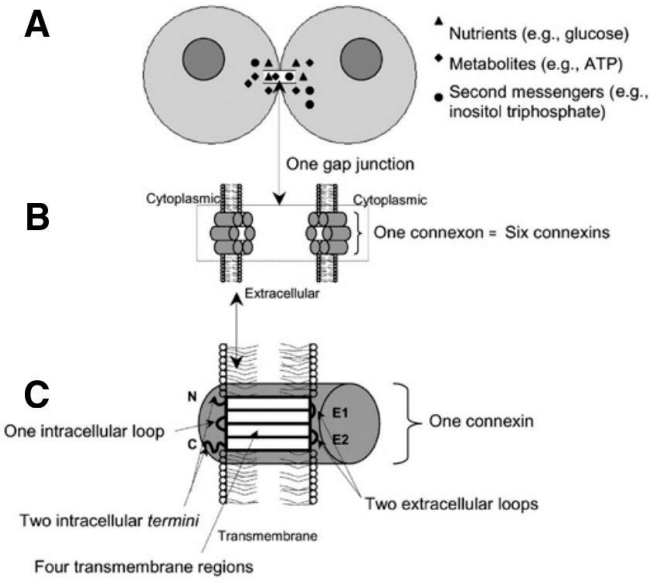

Figure 3.6: Connexin gap junctional intracellular communication (Reprinted with permission from Abbacii 2008)

Cx43 function in ventricular cardiomyocytes is crucial to the overall ability of the heart to contract well; changing the aggregation of Cx43 on the cellular level can lead to arrhythmia and even heart failure (Zhang, Hong, Kléber, Lee, & Shaw, 2014). Cx43 monomers are funneled via dynamic microtubules and the actin cytoskeleton within the cardiomyocyte to allow them to be transported from the Golgi apparatus to the gap junctional plaque at the cellular interface (Zhang et al., 2014). Though cardiomyocytes are able to express connexin proteins at junctions regardless of cellular alignment, multiple studies indicate that the aligned ones have the gap junctional components localized to the longitudinal ends, perhaps better enabling electrical propagation (Khan et al., 2015). Khan et al. found that although the action potential of iPSC-derived cardiomyocytes on flat substrate and aligned on nanofibers were similar, the aligned ones had significantly higher beating rate, indicating improved electrical coupling caused by gap junctional protein aggregation. Within early cardiac embryonic development, Cx45 is present as well as Cx43 (Kehat, Gepstein, Spira, Itskovitz-Eldor, & Gepstein, 2002). This is true for both in vivo and in vitro studies of neonatal rat ventricular cardiomyocytes; while Cx40 (typically found in the atrium and electrical nodes) was not detected, both Cx43 and Cx45 were expressed and colocalized at gap junctional plaques (Darrow, Laing, Lampe, Saffitz, & Beyer, 1995).

Cellular Morphology Influence on Electrophysiology

As mentioned in Chapter 2, the topography of the cell culture substrate influences the morphology and alignment of the cardiomyocytes. Likewise, both of these factors tie into cellular electrophysiology, since the cell has a tightly integrated and elaborate system

where all factors intertwine and affect one another. In hearts treated with microtubule stabilizers, stretch-related arrhythmias are more likely to occur, because the actin cytoskeleton is deeply involved with ion channel activity (McCain & Parker, 2011). Aligned neonatal rat ventricular CMs were found to have higher expression of calcium channel α1C subunit, I_{Na}, and I_{Ca} compared to the non-aligned control (McCain & Parker, 2011). Myocyte size influences propagation just as much as if not more than gap junctional localization (McCain & Parker, 2011).

Influence of Cardiomyocyte Alignment on Electrophysiology

In vitro cardiomyocyte alignment using photolithographic topography formation and adult mouse cardiomyocytes have resulted in action potentials and conduction velocities comparable to that of *in vivo* adult mouse myocardium (McDevitt et al., 2002).

McDevitt et al. used laminin patterning to align rat neonatal cardiomyocytes *in vitro*; this led to the aggregation of connexin43 (Cx43) at the longitudinal ends, indicating the presence of intercalated discs and thus electrochemical cohesion between cells. However, within this study the un-patterned cells had Cx43 present at weak concentrations all along the circumference of the cells.

Electrophysiology Quantification

A popular method of studying cardiac cellular electrophysiology is the patch clamp method. This is a very precise method that allows for measurements of electrical conductance at the membrane. Although dual clamp gap junctional studies are advantageous because they run on an extremely sensitive system that can be attenuated to

specific cells, these are also limited in that intercellular current measurements may not accurately indicate their electrical conductance; gap junction permeability is influenced by the kinetics of molecular transfer (Abbaci, Barberi-Heyob, Blondel, Guillemin, & Didelon, 2008). This method is also unable to examine action potential propagation or conduction velocity, and requires highly technical expertise to collect reliable data (Natarajan et al., 2011; Sigg et al., 2010).

Fluorescence recovery after bleaching (FRAP) microscopy staining may be used; this is another means of identifying the presence of electrical junctions between cells.

Alternatively, microelectrode arrays (MEA) may be used to quantify multicellular electrophysiology. MEA uses an array of electrodes to map out the initiation and propagation of impulses through electrically excitable cell cultures (Kehat et al., 2004). This method can be used to quantitively measure action potential and conduction velocity; it has been used extensively to examine the effect of toxins in cardiac drugs and pesticides on cardiomyocytes (Natarajan et al., 2011).

Lastly, the use of potentiometric and calcium cycling dyes are popular for looking at real-time cardiomyocyte electrophysiology. Potentiometric dyes that correlate directly with voltage were developed a few decades ago after they were found to result in highly similar data to microelectrode recordings; they were highly useful for a wide variety of applications, being useful in subcellular, monocellular, multicellular, and whole heart applications (Todd J. Herron, Peter Lee, 2012). Popular potentiometric dyes include di-

4-ANEPPS and di-8-ANEPPS, fast-response styryl dyes that detect voltage changes in microseconds (Todd J. Herron, Peter Lee, 2012).

Calcium cycling dyes attach to calcium ions that circulate through cells during the excitation-contraction cycle. Due to calcium's role in the excitation-contraction cycle, this produces insightful data about the ability of cells to facilitate this process.

Often, voltage and calcium measures are often measured simultaneously in *in vitro* studies, to compare the effects of pharmaceuticals and condition changes on the two aspects, both intimate elements of cardiac electrophysiology (Hund & Rudy, 2004). The ability to do so is due to advancements in fluorescent dyes, filters, and LED illumination; for example, using a calcium and voltage dye with the same excitation wavelength but different emission wavelengths allows for easy stimulation of the dyes to collect concurrent data (Herron et al., 2012).

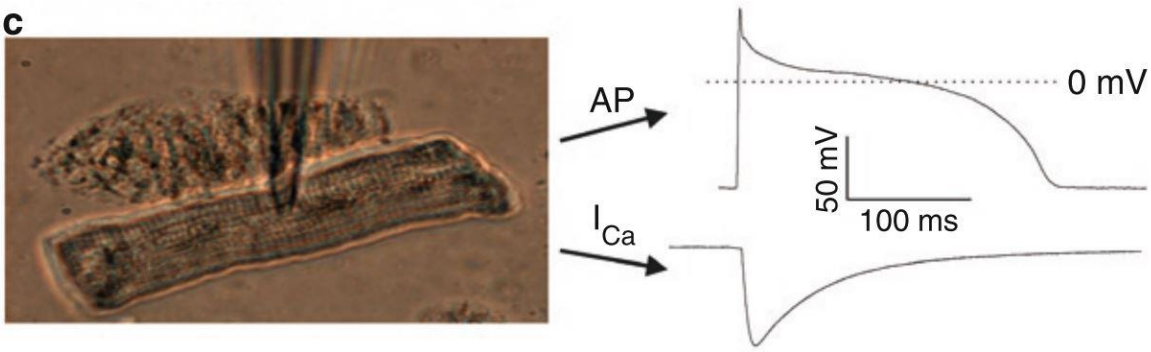

Figure 3.7. Whole cell patch clamp measurement simultaneously recording action potential voltage and inward L-type Ca2+ current (Reprinted with permission from Sigg 2010)

Calcium-Sensitive Dyes

Because calcium ion transport is essential to the excitation-contraction cycle of cardiomyocytes and the action potential, this element is a helpful indicator for studying cellular electrophysiology and the one we selected to explore closely. Changes in intracellular calcium ion release can cause arrhythmia and changes in the excitation-contraction cycle in both in vivo and in vitro cardiomyocytes (Prajapati & Po, 2018). Optical mapping has higher throughput than using the patch clamp technique, and also gives spatial information (Herron et al., 2012). Changes in calcium with use of indicator dyes displays the intake and release of calcium into the sarcoplasmic reticulum (Prajapati & Po, 2018).

There is a perceivable correlation between the parameters of cardiomyocyte action potential and calcium transients, as observed by Prajapati et al. with characterizing hiPSC-CM electrophysiology. They simultaneously measured calcium transients along with voltage using patch clamp to compare the recordings. A high correlation was found between the two parameters (Ca transient to 50% decay and action potential duration to 50% decay had a correlation of $r^2 = 0.92$).

One family of calcium-sensitive dyes are single-wavelength indicators – these have a shift in fluorescence emission when calcium is detected. These are optimal for looking at relative changes in calcium concentration, because there are larger differences in fluorescence intensities in adjacent cells, making it difficult to discern calcium concentration discrepancies from uneven indicator loading (Bootman, Rietdorf, Collins, Walker, & Sanderson, 2014). This discrepancy can be minimized by examining the

fluorescence signal relative to the original signal, represented by $\Delta F/F_0$ (Bootman et al., 2014).

High affinity dyes such as Fluo-4, Fluo-3, and Fura-2 may be chelators and prolong hold onto calcium ions, lengthening the calcium transient and skewing data collected (Todd J. Herron, Peter Lee, 2012). These were developed to specifically and reversibly bind to Ca2+ ions, without high likelihood of binding to other cations like protons and magnesium; they were also developed to become permeable by being stored in acetoxymethyl (AM) ester (Broyles, Robinson, & Daniels, 2018).

Fluo-4

Fluo-4 is a non-ratiometric dye with high affinity for calcium. It was developed to by brighter than former dyes, so that lower concentrations are needed for dynamic imaging of myocytes; this advancement in brightness allowed for transition to use of higher speed cameras, gaining spatial information (Broyles et al., 2018) Fluo-4 is typically stored in acetoxymethyl ester (AM), which allows the dye to more easily permeate the cell membrane (Guatimosim, Guatimosim, & Song, 2011). Once inside the cell, the esterases cleave off the AM group from the dye (Guatimosim et al., 2011).

Monolayer Optical Mapping

Monolayer optical mapping provides challenges not considered in tissue mapping. For example, because neonatal rat cardiomyocytes form monolayers about 5-10 um thick, this may be difficult for finding a matching depth-of-field with the lens used. The PDMS may also be too thick to image through, and samples cannot be inverted because imaging

must be done while the cells are in solution. To account for this, a non-inverted microscope will be used so that imaging is from above the cells with no hinderance to depth-of-field by the substrate.

Electrical Stimulation

Electrode material is typically selected based on ability to conduct electricity in fluid without leaching, usually materials such as gold, platinum, copper, and carbon. Platinum electrodes were first attempted with an Arduino program, with no success in stimulating the culture. The platinum rods were switched to carbon rods which was able to stimulate cells over extended periods of time even at room temperature.

Materials and Method

Substrate Preparation

Cell culture walls are made out of PDMS, making the entire construct comprised of PDMS, thus autoclavable to ensure sterility. If the substrate is reused for another study, it is cleaned by running twice through an ultrasound cleaner in cleanser (Alconox, Inc., White Plains, NY), then once in Milli-Q deionized water (MilliporeSigma, Burlington, MA). This is then autoclaved to sterilize the construct before cell seeding. Cell culture protocols are unchanged from Chapter 2.

Calcium Imaging

Cell cultures at 5-6 days old were used for measuring calcium transients, due to satisfactory maturation of cellular elements at this age. The calcium imaging kit (Thermo

Fisher Scientific, Waltham, MA) includes Fluo-4, AM in DMSO, PowerLoad™ concentrate, and probenecid. 90 nM probenecid is added to retain the dye within the cytosol. Fluo-4 is diluted in Tyrode's solution (HiMedia Laboratories, LLC, West Chester, PA) and incubated in 15 minutes at 37°C and then 15 minutes at room temperature. The sample was then rinsed with warmed PBS and Tyrode's solution was added; this is left at 37°C for 20 more minutes to allow for the indicator to de-esterify.

The LUMPlanFL 60x water immersion objective (Olympus Life Science, Waltham, MA) is used with Axioskop 2 plus microscope (Carl Zeiss Microscopy GmbH, Jena, Germany) using an AxioCam HSm camera (Carl Zeiss Microscopy GmbH, Jena, Germany). The cells are electrically stimulated using a 4011A function generator (B&K Precision Corporation, Yorba Linda, CA) at 1 Hz via a pair of extracellular carbon rod electrodes (GSC International, Inc., Nixa, Missouri) at 5 V with a biphasic pulse, to avoid electrode polarization. The electrical stimulation is verified by a TDS 2014 oscilloscope (Tektronix, Inc., Beaverton, OR). Samples stimulated at 0.3 Hz used an AFG1062 Arbitrary Function Generator (Tektronix, Inc., Beaverton, OR) instead, which had higher precision to control the duty cycle of a longer frequency; all other parameters apart from frequency remained the same. Electrodes are positioned perpendicular to the grooves and wrinkles, so that the flow of the pulse runs along the longitudinal axis of the cardiomyocytes. The cells are imaged in Tyrode's solution; samples are filled to maximum volume of Tyrode's solution to minimize oxygen and osmolarity changes from evaporation over time.

Ca^{2+} Imaging

Cells selected for data collection are not beating simultaneously but beat immediately upon application of electrical stimulation. They are selected regardless of extent of perceived alignment.

The PDMS sample was placed above a glass microscope slide and mounted onto the stage of the microscope. All imaging is performed at room temperature. The images (328x244 pixels, 16-bit resolution, .tif format) are collected at maximum video rate (10 Hz) and saved for further analysis. For consistency, image sets were taken at an exposure time of 10 ms. The videos were taken at maximum speed (usually approximately 7-9 fps) for durations of either 3 or 10 seconds to fully capture the calcium transient pattern. Traces were scaled as change in fluorescence relative to baseline, expressed as F/F_0.

Data analysis of Fluo-4 results was done on ImageJ (NIH). The tifs were compiled into stacks for each time sequence. Fluorescence intensity was measuring at points along an imaginary longitudinal axis line of each cell and plotted over time. This data is converted to express change in Ca^{2+} signal as $\Delta F/F_0$ and frames are converted into seconds.

Results

Neonatal cells culture on grooved substrate were the first to be recorded for calcium cycling, as shown in Graph 3.1. These were stimulated at 1 Hz and recorded for 3 seconds each. Clear cyclic change in fluorescence is observed, but not the full calcium transient curve.

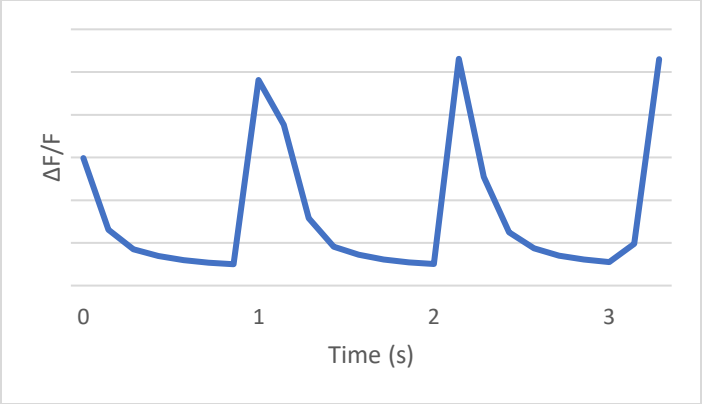

Graph 3.1: Representative Fluo-4 signal of grooved-aligned neonatal cardiomyocytes, triggered at 1 Hz and recorded for 3 seconds.

This was compared to cardiomyocytes culture on wrinkles, which were treated in identical fashion to the grooves except recording time was extended to 10 seconds to better capture the calcium transient consistency, as seen in Graph 3.2.

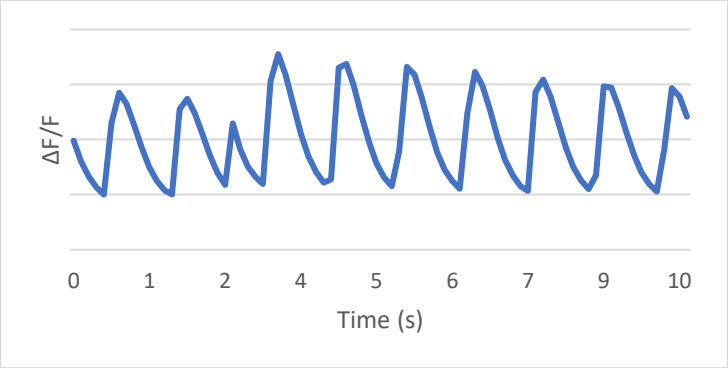

Graph 3.2: Representative Fluo-4 signal of cardiomyocytes cultured on wrinkles, triggered at 1 Hz and recorded for 10 seconds.

The transient was also explored in control cell culture, grown on flat PDMS. This was also recorded 10 seconds long, shown below in Graph 3.3.

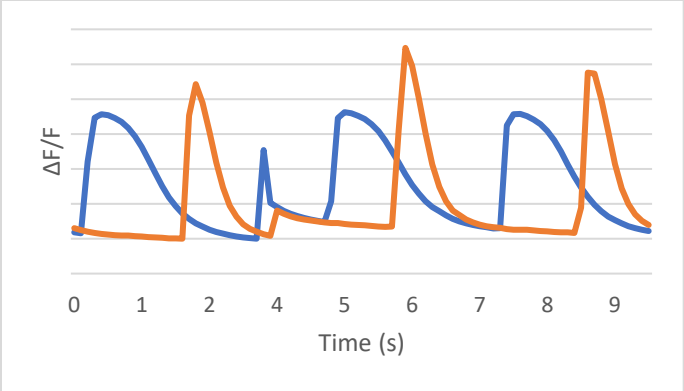

Graph 3.3: Representative Fluo-4 calcium transients of neonatal cardiomyocytes cultured on flat PDMS, stimulated at 1 Hz and recorded for 10 seconds.

We found it peculiar that even though the calcium transient of the control cells were delayed and did not occur at every stimulation, they had a more accurate calcium transient curve indicating improved development. Thus, we repeated the Fluo-4 dye studies but at 0.3 Hz (slowed down to the rate of cycling of these control cultures) to observe whether this affected the data for either grooves, wrinkles, or control.

Below in Graph 3.4, the transient of the wrinkle culture in at 0.3 Hz stimulation are shown.

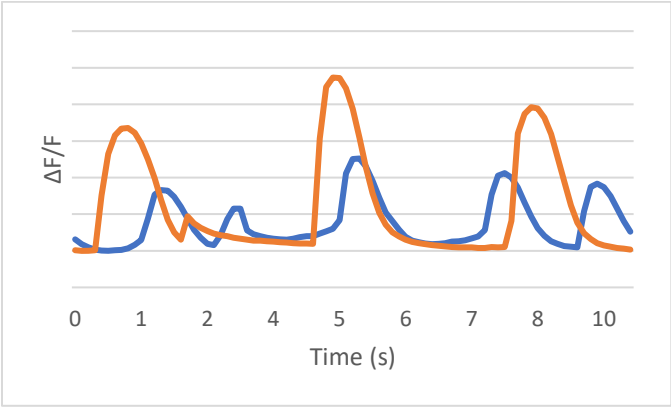

Graph 3.4: Representative Fluo-4 calcium signals of neonate cardiomyocytes cultured on wrinkled substrate, stimulated at 0.3 Hz with a longer pulse and recorded at 10 Hz.

We noted that these observed cells under fluorescence had irregular sparking behavior and concluded that it was due to the stimulation pulse being too prolonged, due to the limitations of the function generator. This was suspected of disrupting electrical signals in cardiomyocytes. Thus, we continued with using a different, more precise function generator for the remainder of the studies. The control culture was stimulated at 0.3 Hz for the calcium transients in in all following figures.

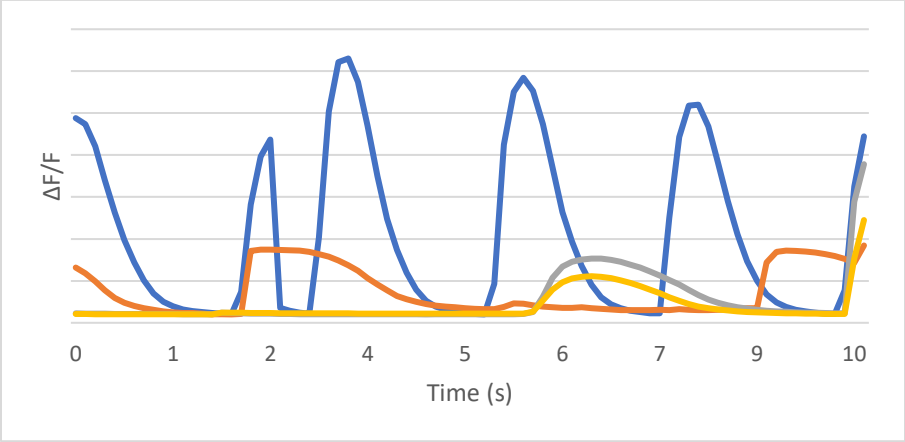

Graph 3.5: Representative Fluo-4 calcium transients of neonate cardiomyocytes cultured on flat PDMS (control)

The control cell culture seems to have beating at 0.3 Hz, though still not with the same consistency as aligned cells. As can see from Figure 3.5, some cells are able to recapitulate the calcium spikes at the correct frequency of efficient cycling. However, this is due to the fact that in random culture some cells are expected to be more aligned by chance. These are not within the same direction though, and most cells do remain relatively inefficient at calcium cycling for the control culture.

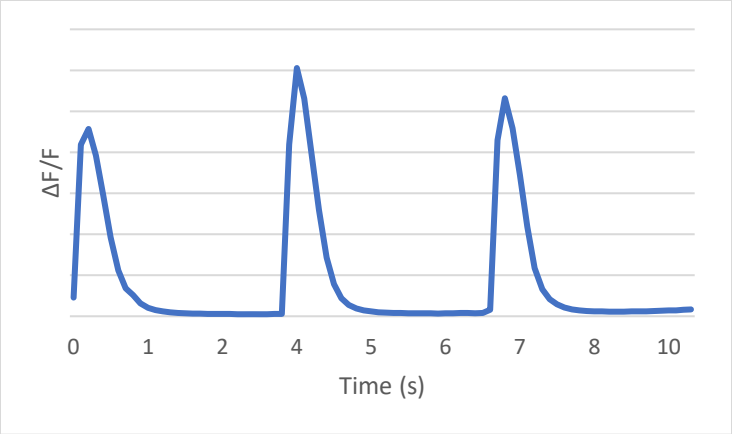

Graph 3.6: Representative calcium transient of neonate cardiomyocytes cultured on grooved PDMS

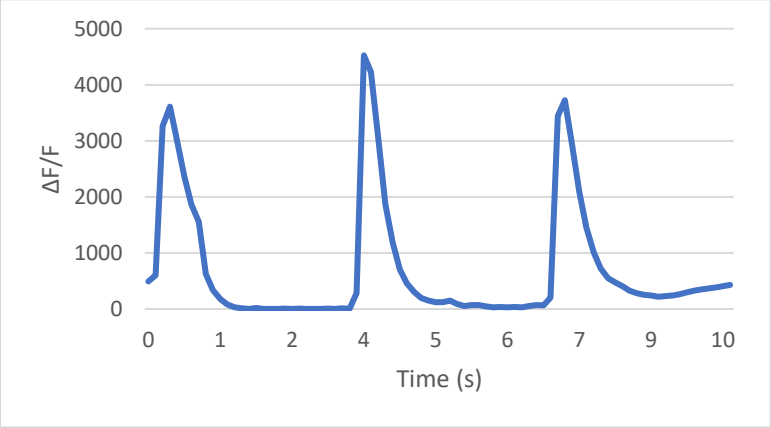

Graph 3.7: Representative calcium transient of neonate cardiomyocytes cultured on wrinkled PDMS

The experiments on aligned cultures, both on wrinkles and grooves, were successful in capturing the sharp calcium transient of matured cardiomyocytes. Interestingly, this occurs even in cells that do not individually align well individually despite being cultured on aligned microtopography.

Calcium Transients Along Cells

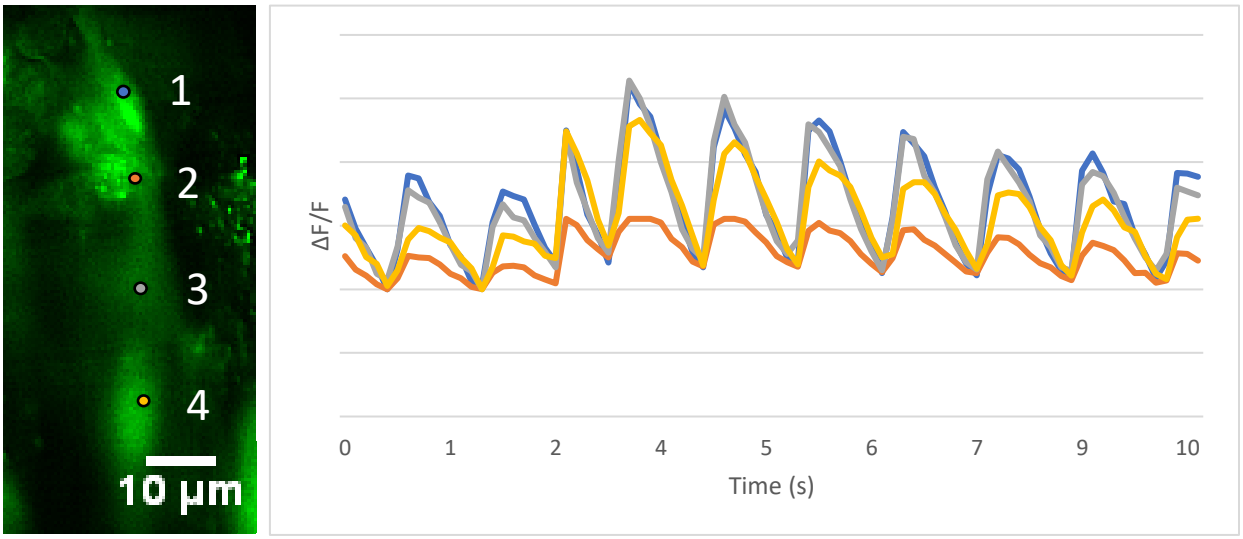

Graph 3.8: Calcium transients along aligned cells

We wanted to explore whether the calcium cycling had any sort of time delay along the longitudinal axis of aligned cells. Though the curves were varying in amplitude, the frequency and timing of the profile did not change within the cell location.

Calcium Flux Consistency

We calculated how often the culture was able to facilitate calcium flux for every stimulation pulse. At 1 Hz the aligned cultures were able to consistently keep up, but the control only successfully cycled calcium about a third of the time. For 0.3 Hz stimulation, grooves and wrinkles continued to successfully cycle at every pulse. For the control at 0.3 Hz, although the average was close to 100%, you can see in Figure 19 that the standard deviation is extremely high, with both samples stimulating only on some of the pulses as well as cultures that contracted in between pulses, indicating possible reentry due to the prolonged pulse.

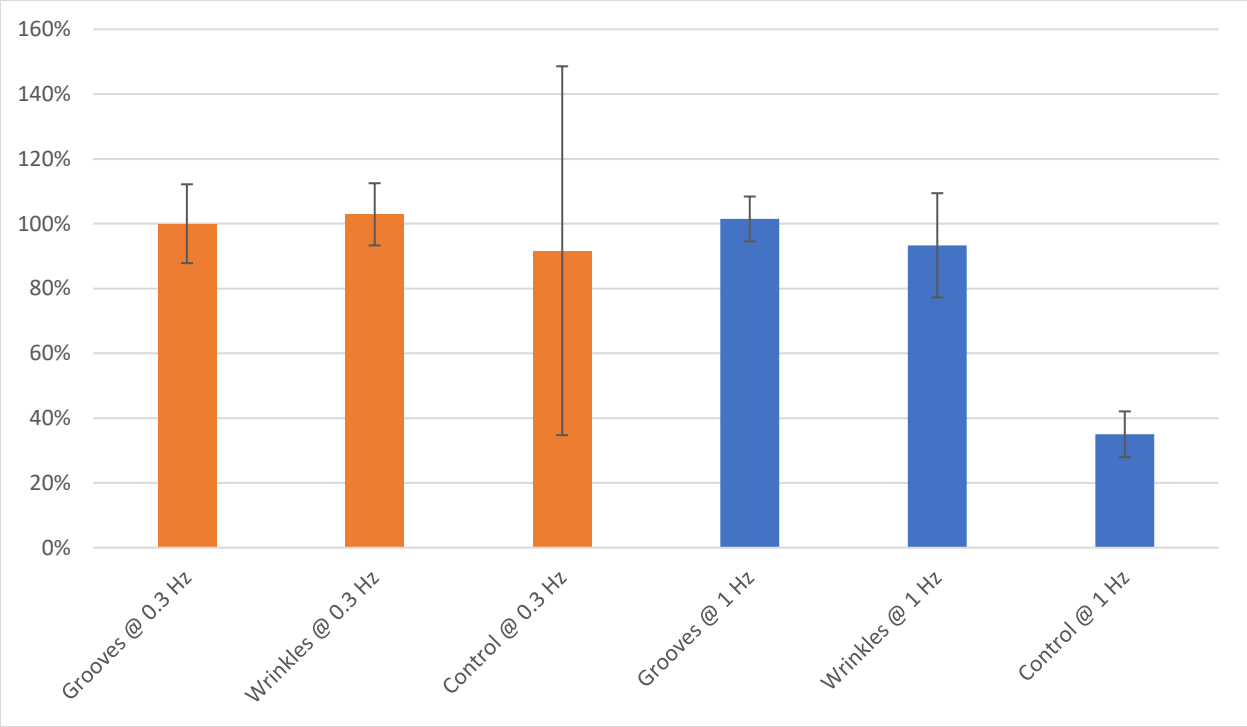

Graph 3.9: Ratio of pulse stimulation to calcium flux in culture, as a percentage. Orange bars are at 0.3 Hz and blue bars are at 1 Hz. Error bars shown are of standard deviation.

Peak-to-Peak Time

We measured the time difference between peaks for wrinkles, grooves, and control, all at 0.3 Hz stimulation frequency. In theory, this should mean that a perfect calcium transient that is able to react to every stimulation pulse should be approximately 3.33 seconds long. Below in Table 1 are our results:

	Peak-to-Peak Time (s)	Sample Size
Grooves	3.183±0.544	30
Wrinkles	3.281±0.446	46
Control	2.881±1.601	9

Table 3.1: Average peak-to-peak times of neonatal cardiomyocytes cultured on grooves, wrinkles, and flat PDMS

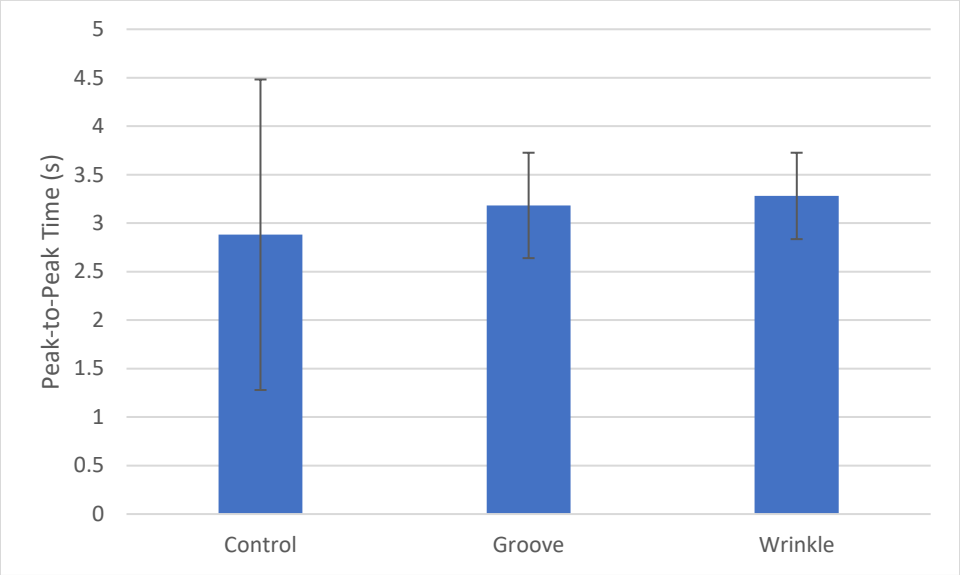

Graph 3.10: Average peak-to-peak durations of cultures stimulated at 0.3 Hz

Cell Response to Changing Stimulation Frequency

We attempted to record the same cell at different frequencies of stimulation, but none were successful in surviving the first recording long enough to sustain beating at a different frequency, potentially due to photobleaching.

Discussion

Stimulation

Our initial calcium studies were attempted with platinum electrodes with no success. Although not focused on platinum electrodes, Tandon & Marsano found that carbon electrodes were optimal compared to stainless steel and titanium ones. They have

high resistance to corrosion as well as capacitance, and have been used in cardiac tissue engineering with satisfactory charge transfer behavior (Tandon & Marsano, 2011).

Short pulses, like as the 1 ms duration we chose, minimizes the odds of pH gradients and the extent to which the cells are exposed to the electric field (Tandon & Marsano, 2011). Biphasic pulses may potentially inhibit action potential because the second pulse is hyperpolarizing and can affect AP initiation (Tandon & Marsano, 2011).

Fluo-4 Dye

AM ester in the Fluo-4 dye preparation may hydrolyze, creating formaldehyde, protons, and acetic acid (Broyles et al., 2018). When loading the AM ester at a high temperature into cells, this can cause the indicator to strongly favor compartmentalizing subcellularly, thus affecting cytosolic calcium ion measurements (Guatimosim et al., 2011).

Indicators can leak from the cytosol to the extracellular area, caused by anion transport systems (Takahashi, Camacho, Lechleiter, & Herman, 1999). After observing this in preliminary fluorescence studies, probenecid was added to minimize this effect for shown data.

Another factor to consider is that the indicators tend to get compartmentalized, which means that they get trapped within intracellular organelles and thus skews the distribution within the cell (Takahashi et al., 1999). This was observed in cells that were imaged for longer periods of time.

Neonatal Vs. Adult Calcium Cycling

The use of neonatal cardiomyocytes in contrast to adult cells likely had a significant effect on the electrical properties. This is primarily because of the discrepancies in the distribution of gap junctions – adult ventricular cardiomyocytes have these localized strongly at the longitudinal ends, whereas neonatal cells will have these distributed around cell borders (Spach, Heidlage, Dolber, & Barr, 2000). Neonatal cells also have a larger surface to volume ratio, being less rod-like in geometry compared to adult cells (Fast & Kleber, 1993).

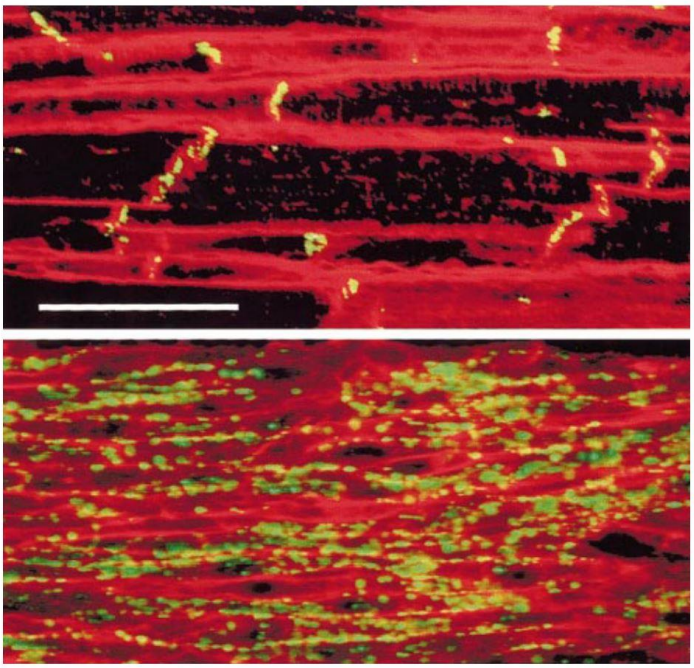

Figure 3.11: Distribution of connexin 43 (green) in adult (above) vs. neonatal (below) canine ventricular cardiomyocytes. Scale bar is 50 um (Reprinted with permission from Spach 2000).

The electrical resistance between a pair of adult ventricular cardiomyocytes is 2 MΩ, while for 2-day-old neonatal cells is 30 MΩ; while we can come to the conclusion

that the resistance of an older and theoretically further matured neonatal culture, it would still be significantly higher than that of the mature cells (Fast & Kleber, 1993).

IP-3 Pathway

The inositol-triphosphate (IP3) pathway is a known means of electrical conduction in neonatal and stem cell-derived cardiomyocytes, but also interestingly in failing adult human cardiomyocytes (Kane, Couch, & Terracciano, 2015; Poindexter, Smith, Buja, & Bick, 2001).

Blockage of the IP-3 pathway in electrically stimulated neonatal cardiomyocytes led to poorly synchronized and localized contractions, indicating lack of contractile protein organization (Radisic et al., 2004). When L-type VOCCs or RyRs were blocked in neonatal cardiomyocytes, intercellular communication was not found to be affected significantly; on the other hand, if the IP3 pathway was inhibited calcium signals as prominently as if gap junctions were removed (Li et al., 2012). This is interpreted as the IP3 pathway being intertwined somehow with Cx43-regulated calcium ion movement (Li et al., 2012). IP3 calcium sparks are found to be concentrated around the nucleus, largely independent from RyR induced CICR, despite being simultaneous in transients (Luo et al., 2008). This is due to the nuclear envelope, along with its protrusions into the nucleus, are the nuclear calcium storage sites (Luo et al., 2008).

Mitochondrial Calcium

The role of mitochondrial calcium in cardiomyocytes is highly debated within the scientific community. Contrasting evidence exists for whether mitochondria partake in

calcium cycling actively via ATP production or passively through buffering calcium ion transients within the cytoplasm (Kane et al., 2015). There is evidence that when mitochondrial Ca transients were suppressed, this increased the cell's overall transient by 50-60%, indicating that the mitochondrial calcium movement may buffer the cell transient (Eisner et al., 2017). Mitochondrial calcium movement is a prominent factor in regulating the IP3 pathway's calcium release in oocytes, though no research is published on its role in cardiomyocytes (Landgraf, Gellerich, & Wussling, 2004). However, mitochondria uncoupling has links to swift reduction of cytosolic calcium removal in cardiomyocytes (Landgraf et al., 2004).

Conclusion

Based on our studies comparing calcium flux between grooved, wrinkled, and flat PDMS, we can conclude that substrate topography does in fact allow for the neonatal cell culture to cycle calcium more efficiently, regardless of the individual cells' alignment or position relative to other cells. Both aligned cultures were able to consistently cycle calcium along with electrical stimulation of different frequencies, while the control culture was much more erratic regardless of frequency. The aligned cultures also had much more consistent peak-to-peak times in line with the pulse frequency, indicating their enhanced physiological maturity allowing for quick and efficient calcium cycling for the excitation-contraction cycle.

References

Abbaci, M., Barberi-Heyob, M., Blondel, W., Guillemin, F., & Didelon, J. (2008). Advantages and limitations of commonly used methods to assay the molecular permeability of gap junctional intercellular communication. *BioTechniques*, *45*(1), 33–62. https://doi.org/10.2144/000112810

Bers, D. M. (2008). Calcium Cycling and Signaling in Cardiac Myocytes. *Annual Review of Physiology*, *70*, 23–49. https://doi.org/10.1146/annurev.physiol.70.113006.100455

Bootman, M. D., Rietdorf, K., Collins, T., Walker, S., & Sanderson, M. (2014). Ca2+ Sensitive Fluorescent Dyes and Intracellular Ca 2 + Imaging. In J. B. Parys, M. Bootman, D. I. Yule, & G. Bultynck (Eds.), *Calcium Techniques: A Laboratory Manual* (pp. 25–50). Cold Spring Harbor Laboratory Press. https://doi.org/10.1101/pdb.top066050

Broyles, C. N., Robinson, P., & Daniels, M. J. (2018). Fluorescent, Bioluminescent, and Optogenetic Approaches to Study Excitable Physiology in the Single Cardiomyocyte. *Cells*, *7*(51), 1–28. https://doi.org/10.3390/cells7060051

Darrow, B. J., Laing, J. G., Lampe, P. D., Saffitz, J. E., & Beyer, E. C. (1995). Expression of Multiple Connexins in Cultured Neonatal Rat Ventricular Myocytes Darrow,. *Circulation Research*, *76*(3), 381–387.

Eisner, D. A., Caldwell, J. L., Kistamás, K., & Trafford, A. W. (2017). Calcium and Excitation-Contraction Coupling in the Heart. *Circulation Research*, *121*(2), 181–195. https://doi.org/10.1161/CIRCRESAHA.117.310230

Fast, V. G., & Kleber, A. G. (1993). Microscopic Conduction in Cultured Strands of Neonatal Rat Heart Cells Measured With Voltage-Sensitive Dyes. *Circulation Research*, *73*(5), 914–925.

Fearnley, C. J., Roderick, H. L., & Bootman, M. D. (2011). Calcium Signaling in Cardiac Myocytes. *Cold Springs Harbor Perspectives in Biology*, 1–20.

Goodenough, D. A., & Paul, D. L. (2009). Gap Junctions. *Cold Springs Harbor Perspectives in Biology*, 1–19.

Guatimosim, S., Guatimosim, C., & Song, L.-S. (2011). Imaging Calcium Sparks in Cardiac Myocytes. *Methods Mol BIol*, *689*, 205–214. https://doi.org/10.1007/978-1-60761-950-5

Herron, T. J., Lee, P., & Jalife, J. (2012). Optical Imaging of Voltage and Calcium in Cardiac Cells & Tissues. *Circulation Research*. https://doi.org/10.1161/CIRCRESAHA.111.247494

Hund, T. J., & Rudy, Y. (2004). Rate Dependence and Regulation of Action Potential and Calcium Transient in a Canine Cardiac Ventricular Cell Model. *Circulation*, *110*,

3168–3174. https://doi.org/10.1161/01.CIR.0000147231.69595.D3

Hwang, H. S., Kryshtal, D. O., Feaster, T. K., Sánchez-freire, V., Zhang, J., Kamp, T. J., … Knollmann, B. C. (2015). Comparable calcium handling of human iPSC-derived cardiomyocytes generated by multiple laboratories. *Journal of Molecular and Cellular Cardiology*, *85*, 79–88. https://doi.org/10.1016/j.yjmcc.2015.05.003

Kane, C., Couch, L., & Terracciano, C. M. (2015). Excitation – contraction coupling of human induced pluripotent stem cell-derived cardiomyocytes. *Frontiers in Cell and Developmental Biology*, *3*, 1–8. https://doi.org/10.3389/fcell.2015.00059

Kanno, S., & Saffitz, J. E. (2001). The role of myocardial gap junctions in electrical conduction and arrhythmogenesis. *Cardiovascular Pathology*, *10*, 169–177.

Kehat, I., Gepstein, A., Spira, A., Itskovitz-eldor, J., & Gepstein, L. (2002). High-Resolution Electrophysiological Assessment of Human Embryonic Stem Cell–Derived Cardiomyocytes, 659–661. https://doi.org/10.1161/01.RES.0000039084.30342.9B

Kehat, I., Khimovich, L., Caspi, O., Gepstein, A., Shofti, R., Arbel, G., … Gepstein, L. (2004). Electromechanical integration of cardiomyocytes derived from human embryonic stem cells. *Nature Biotechnology*, *22*(10), 1282–1289. https://doi.org/10.1038/nbt1014

Khan, M., Xu, Y., Hua, S., Johnson, J., Belevych, A., Janssen, P. M. L., … Angelos, M. G. (2015). Evaluation of Changes in Morphology and Function of Human Induced Pluripotent Stem Cell Derived Cardiomyocytes (HiPSC-CMs) Cultured on an Aligned-Nanofiber Cardiac Patch. *PLoS ONE*, 1–20. https://doi.org/10.1371/journal.pone.0126338

Kleber, A. G., & Rudy, Y. (2004). Basic Mechanisms of Cardiac Impulse Propagation and Associated Arrhythmias. *Physiol Rev*, *84*, 431–488.

Kleber, A. G., & Saffitz, J. E. (2014). Role of the intercalated disc in cardiac propagation and arrhythmogenesis. *Frontiers in Physiology*, *5*(OCT), 1–9. https://doi.org/10.3389/fphys.2014.00404

Landgraf, G., Gellerich, F. N., & Wussling, M. H. P. (2004). Inhibitors of SERCA and mitochondrial Ca-uniporter decrease velocity of calcaium waves in rat cardiomyocytes. *Molecular and Cellular Biochemistry*, *256–257*(1–2), 379–386. https://doi.org/10.1023/b:mcbi.0000009883.71379.51

Li, C., Meng, Q., Yu, X., Jing, X., Xu, P., & Luo, D. (2012). Regulatory Effect of Connexin 43 on Basal Ca 2 + Signaling in Rat Ventricular Myocytes. *PLoS ONE*, *7*(4), 1–10. https://doi.org/10.1371/journal.pone.0036165

Luo, D., Yang, D., Lan, X., Li, K., Li, X., Chen, J., … Cheng, H. (2008). Nuclear Ca sparks and waves mediated by inositol 1,4,5-triphosphate receptors in neonatal rat

cardiomyocytes. *Cell Calcium*, *43*, 165–174.

Macfarlane, P., van Oosterom, A., Pahlm, O., Kligfield, P., Janse, M., & Camm, J. (2010). *Comprehensive Electrocardiology*. *Comprehensive Electrocardiology* (Vol. 1). https://doi.org/10.1007/978-1-84882-046-3

Manring, H. R., Dorn, L. E., Ex-willey, A., Accornero, F., & Ackermann, M. A. (2018). At the heart of inter- and intracellular signaling : the intercalated disc. *Biophysical Reviews*, *10*, 961–971.

McCain, M. L., & Parker, K. K. (2011). Mechanotransduction: The role of mechanical stress, myocyte shape, and cytoskeletal architecture on cardiac function. *European Journal of Physiology*, *462*, 89–104. https://doi.org/10.1007/s00424-011-0951-4

McDevitt, T. C., Angello, J. C., Whitney, M. L., Reinecke, H., Hauschka, S. D., Murry, C. E., & Stayton, P. S. (2002). In vitro generation of differentiated cardiac myofibers on micropatterned laminin surfaces. *J Biomed Mater Res*, *60*, 472–479. https://doi.org/10.1008/jbm.1292

Natarajan, A., Stancescu, M., Dhir, V., Armstrong, C., Sommerhage, F., Hickman, J. J., & Molnar, P. (2011). Patterned cardiomyocytes on microelectrode arrays as a functional, high information content drug screening platform. *Biomaterials*, *32*(18), 4267–4274. https://doi.org/10.1016/j.biomaterials.2010.12.022

Poindexter, B. J., Smith, J. R., Buja, L. M., & Bick, R. J. (2001). Calcium signaling mechanisms in dedifferentiated cardiac myocytes : comparison with neonatal and adult cardiomyocytes. *Cell Calcium*, *30*(6), 373–382. https://doi.org/10.1054/ceca.2001.0249

Prajapati, C., & Po, R. (2018). Simultaneous recordings of action potentials and calcium transients from human induced pluripotent stem cell derived cardiomyocytes. *Biology Open*, *7*, 1–10. https://doi.org/10.1242/bio.035030

Radisic, M., Park, H., Shing, H., Consi, T., Schoen, F. J., Langer, R., … Vunjak-Novakovic, G. (2004). Functional assembly of engineered myocardium by electrical stimulation of cardiac myocytes cultured on scaffolds. *Proceedings of the National Academy of Sciences*, *101*(52), 18129–18134. https://doi.org/10.1073/pnas.0407817101

Rohr, S. (2004). Role of gap junctions in the propagation of the cardiac action potential. *Cardiovascular Research*, *62*, 309–322. https://doi.org/10.1016/j.cardiores.2003.11.035

Severs, N. J., Bruce, A. F., Dupont, E., & Rothery, S. (2008). Remodelling of gap junctions and connexin expression in diseased myocardium. *Cardiovascular Research*, *80*, 9–19. https://doi.org/10.1093/cvr/cvn133

Sigg, D. C. ., Laizzo, P. A. ., Xiao, Y.-F., & He, B. (2010). *Cardiac Electrophysiology*

Methods and Models. *Cardiac Electrophysiology Methods and Models*. https://doi.org/10.1007/978-1-4419-6658-2

Spach, M. S., Heidlage, J. F., Barr, R. C., & Dolber, P. C. (2004). Cell size and communication: Role in structural and electrical development and remodeling of the heart. *Heart Rhythm*, *4*, 500–515.

Spach, M. S., Heidlage, J. F., Dolber, P. C., & Barr, R. C. (2000). Electrophysiological Effects of Remodeling Cardiac Gap Junctions and Cell Size Experimental and Model Studies of Normal Cardiac Growth. *Circ Res.*, *86*, 302–311.

Takahashi, A., Camacho, P., Lechleiter, J. D., & Herman, B. (1999). Measurement of intracellular calcium. *Physiological Reviews*, *79*(4), 1089–1125. https://doi.org/10.1152/physrev.1999.79.4.1089

Tandon, N., & Marsano, A. (2011). Optimization of Electrical Stimulation Parameters for Cardiac Tissue Engineering. *J Tissue Eng Regen Med*, *5*(6), 115–125. https://doi.org/10.1002/term.377.Optimization

Todd J. Herron, Peter Lee, and J. J. (2012). Optical Imaging of Voltage and Calcium in Cardiac Cells & Tissues. *Circ Res.*, *110*(4), 609–623. https://doi.org/10.1161/CIRCRESAHA.111.247494.Optical

Veeraraghavan, R., Gourdie, R. G., & Poelzing, S. (2014). Mechanisms of cardiac conduction : a history of revisions. *Heart Circ Physiol*, *306*, H619–H627. https://doi.org/10.1152/ajpheart.00760.2013

Zhang, S. S., Hong, S. G., Kléber, A. G., Lee, L. P., & Shaw, R. M. (2014). A micropatterning approach for imaging dynamic Cx43 trafficking to cell-cell borders. *FEBS Letters*, *588*(8), 1439–1445. https://doi.org/10.1016/j.febslet.2014.01.002

Zheng, H., Liu, S., Tian, W., Yan, H., Zhang, Y., & Li, Y. (2012). A three-dimensional in vitro culture model for primary neonatal rat ventricular myocytes. *Current Applied Physicas*, *12*, 826–833. https://doi.org/10.1016/j.cap.2011.11.014

Zhu, C., Rodda, A. E., Truong, V. X., Shi, Y., Zhou, K., Haynes, J. M., … Forsythe, J. S. (2018). Increased Cardiomyocyte Alignment and Intracellular Calcium Transients Using Micropatterned and Drug-Releasing Poly(Glycerol Sebacate) Elastomers. *ACS Biomaterials Science and Engineering*, *4*(7), 2494–2504. https://doi.org/10.1021/acsbiomaterials.8b00084

CHAPTER 4

FUTURE RECOMMENDATIONS

Stem Cell Usage

Embryonic stem cells from mammalian blastocysts have been successfully differentiated to cardiomyocytes for drug screening and also transplantation one day. mESCs differentiated to cardiomyocyte clusters have been found to increase Cx43 expression in line with an increase in conduction velocity as well, mirroring the developing in vivo within mouse embryonic hearts (Sigg, Laizzo, Xiao, & He, 2010). Additionally, hESC-CMs have been found to electrically integrate with primary neonatal rat CMs within one day as recorded via MEA in a co-culture model (Sigg et al., 2010). hESCs have successfully been induced at least partially into cardiomyocytes using wrinkled substrates, creating spontaneously beating embryoid bodies (Baum, Panther II, Khine, & McCloskey, 2011).

In terms of personalized medicine, if iPSCs can be derived from patients then they could theoretically have the same genetics and respective response to pharmaceutics as the native cells of the patient (Knight, Grosberg, & McCain, 2015).

Long Term Electrical Stimulation

Electrical stimulation during cell culture has been shown to lead to matured intercalated discs and sarcomeres, as well as higher density of desmosomes, which connect to actin to strengthen mechanical cohesion (Tandon & Marsano, 2011). When

initiated at the correct time (3 days after seeding for 3D cultures, 24 hours for 2D), long term electrical stimulation can encourage functional maturation of neonatal cardiomyocytes (Tandon et al., 2009).

Long term electrical stimulation of *in vitro* neonatal cardiomyocytes for 8 days was found to produce sarcomeric volume fraction similar to those of neonatal ventricles, but nonstimulated cultures did not have well organized or aligned sarcomeres (Tandon et al., 2009). Stimulation has also been shown to increase glycogen levels and organized mitochondria between myofibrils in cardiomyocytes (Tandon et al., 2009).

Co-culture with Non-Myocytes

Non-cardiomyocytes within the heart contribute factors that help develop physiologically optimal behavior in cardiomyocytes. For example, fibroblasts provide paracrine signals and remodel ECM, and endothelial cells also use paracrine factors such as NRG-1, NO, and ET-1; cumulatively, these inputs encourage the cardiomyocytes to contract more strongly, be less vulnerable to cardiotoxic drugs, and mature more robustly, among other effects (Kurokawa & George, 2016). For these reasons, it would be worthwhile to study the effects of cardiomyocytes co-cultured with other cells native to the *in vivo* heart to observe how this affects cardiomyocyte behavior. Although fibroblasts are highly heterogeneous even within a single organ, it would be worthwhile to co-culture with primary cardiac fibroblasts obtained from the same dissection as the primary cardiomyocytes (Kurokawa & George, 2016).

Cardiac fibroblasts in particular have been shown to have membrane potential fluctuations along with electrical stimulation, depolarizing and hyperpolarizing due to sodium ion flow (Tandon & Marsano, 2011). Though not contractile by nature, it would be worth investigating how these affect electrical propagation, particularly if done in tandem with long term electrical stimulation.

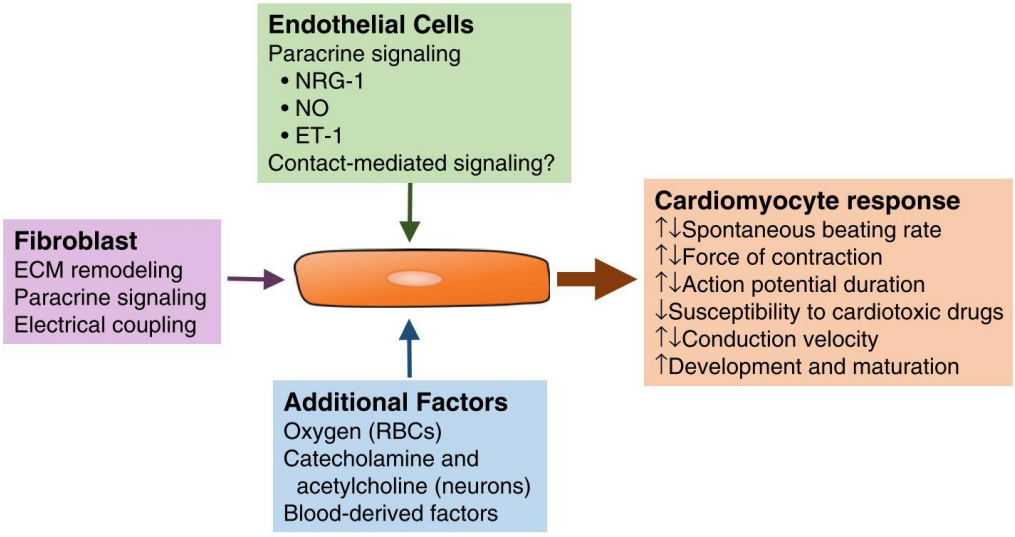

Figure 4.1: Influential factors of non-myocytes within the cardiac environment and their cumulative effects on cardiomyocyte functional maturation (Reprinted with permission from Kurokawa 2016).

Three-Dimensional Culture

Using three-dimensional culture will be advantageous to the two-dimensional culture used in these studies. 3D culture has been found to be higher in α-actinin than 2D (Soares et al., 2012). In other physiological models such as liver and tumor models. 3D cell cultures have been found to have increased drug screening abilities (Kurokawa & George, 2016).

Computational Modeling

More developed in vitro models can be compared to computation models of ventricular myocyte calcium cycling. An example of modeling is creating a coupled calcium release unit network, where each unit contains a pre-determined number of L-type calcium channels as well as ryanodine receptors (Nivala et al., 2012).

Multi-Parametric Measurements

Measuring calcium movement alongside voltage would be insightful to cell functionality, due to the intimate coupling between the calcium transient and the action potential. One method of doing this would be simultaneous uptake and imaging of calcium and voltage dyes. Other methods to consider for measuring voltage, though non-optical, would be utilizing the patch clamp method or MEAs, though the exact same culture will not be able to be measured simultaneously with calcium using this method.

In addition, observing contraction forces via optical measurements would be worth looking into as well, highlighting the mechanical aspect of the excitation-contraction coupling cycle.

Alternative Substrate Materials

PDMS was an optimal choice for cell culture substrate, and although there are many other options in terms of material to use, within our scope there is no strong argument for exploring other materials due to extensive research conducted on the discrepancies of their properties in biological applications. However, exploring different types of PDMS would be insightful. Many studies on cardiomyocytes are conducted on the same PDMS, Sylgard 184. However, realistically, in vivo ECM has a much softer

substrate with a lower elastic modulus. Since the PDMS we used is approximately 1.72 MPa. In comparison, physiologically the elastic modulus is approximately 15 kPa, much softer than our PDMS (Boothe et al., 2016). It would be insightful to look into how this affects the calcium transients. Van Deel et al. found that on stiffer polyacrylamide, cardiomyocytes had smaller Ca2+ amplitudes and slower propagation velocity compared to softer polyacrylamide gels that were more physiologically similar (van Deel et al., 2017) .

Pharmaceuticals for Exploring Cellular Physiology

Verapamil is a popular drug that blocks calcium channels and minimizes cell ability to contract (Oyunbaatar, Lee, Patil, Kim, & Lee, 2016). These are often used to block simultaneous contractions while still allowing for cell excitability to be maintained (Au, Cui, Chu, Veres, & Radisic, 2009). This can be used to stop beating during culture maturation to observe whether the beating itself has any effect on the cell alignment and functional development.

References

Au, H. T. H., Cui, B., Chu, Z. E., Veres, T., & Radisic, M. (2009). Cell culture chips for simultaneous application of topographical and electrical cues enhance phenotype of cardiomyocytes. *Lab on a Chip*, *9*(4), 564–575. https://doi.org/10.1039/b810034a

Baum, M. L., Panther II, J. B., Khine, M., & McCloskey, K. E. (2011). Aligning cells on wrinkled surface. United States.

Boothe, S. D., Myers, J. D., Pok, S., Sun, J., Xi, Y., Nieto, R. M., … Jacot, J. G. (2016). The Effect of Substrate Stiffness on Cardiomyocyte Action Potentials. *Cell Biochemistry and Biophysics*, *74*(4), 527–535. https://doi.org/10.1007/s12013-016-0758-1

Hwang, H. S., Kryshtal, D. O., Feaster, T. K., Sánchez-freire, V., Zhang, J., Kamp, T. J., … Knollmann, B. C. (2015). Comparable Calcium Handling Of Human iPSC-derived Cardiomyocytes Generated By Multiple Laboratories. *Physiology & Behavior*, *85*, 79–88. https://doi.org/10.1016/j.physbeh.2017.03.040

Knight, M. B., Grosberg, A., & McCain, M. L. (2015). In Vitro Tools for Quantifying Structure - Function Relationships in Cardiac Myocyte Cells and Tissues. In *Cardiac Cytoarchitecture: How to Maintain a Working Heart* (pp. 15–39). Springer International Publishing. https://doi.org/10.1007/978-3-319-15263-9

Kurokawa, Y. K., & George, S. C. (2016). Tissue engineering the cardiac microenvironment: Multicellular microphysiological systems for drug screening. *Advanced Drug Delivery Reviews*, *96*, 225–233. https://doi.org/10.1016/j.addr.2015.07.004

Nivala, M., Lange, E. De, Rovetti, R., Qu, Z., Jafri, M. S., & Mason, G. (2012). Computational modeling and numerical methods for spatiotemporal calcium cycling in ventricular myocytes. *Frontiers in Physiology*, *3*(May), 1–12. https://doi.org/10.3389/fphys.2012.00114

Oyunbaatar, N. E., Lee, D. H., Patil, S. J., Kim, E. S., & Lee, D. W. (2016). Biomechanical characterization of cardiomyocyte using PDMS pillar with microgrooves. *Sensors (Switzerland)*, *16*(8), 1–13. https://doi.org/10.3390/s16081258

Sigg, D. C. ., Laizzo, P. A. ., Xiao, Y.-F., & He, B. (2010). *Cardiac Electrophysiology Methods and Models*. *Cardiac Electrophysiology Methods and Models*. https://doi.org/10.1007/978-1-4419-6658-2

Soares, C. P., Midlej, V., de Oliveira, M. E. W., Benchimol, M., Costa, M. L., & Mermelstein, C. (2012). 2D and 3D-organized cardiac cells shows differences in cellular morphology, adhesion junctions, presence of myofibrils and protein expression. *PLoS ONE*, *7*(5). https://doi.org/10.1371/journal.pone.0038147

Tandon, N., Cannizzaro, C., Chao, P. P.-H. G., Maidhof, R., Marsano, A., Au, H. T. H., … Vunjak-Novakovic, G. (2009). Electrical stimulation systems for cardiac tissue engineering. *Nature Protocols*, *4*(2), 155–173. https://doi.org/10.1038/nprot.2008.183.Electrical

Tandon, N., & Marsano, A. (2011). Optimization of Electrical Stimulation Parameters for Cardiac Tissue Engineering. *J Tissue Eng Regen Med*, *5*(6), 115–125. https://doi.org/10.1002/term.377.Optimization

APPENDICES

Appendix A

PDMS Wrinkled Membrane Fabrication Protocol

Purpose: Polydimethylsiloxane (PDMS), a silicone material, is fabricated to have contoured wrinkles for cardiomyocyte alignment in cell culture.

Materials:
Sylgard 184 Silicone Encapsulant Base (Dow Corning, 4019862)
Sylgard 184 Silicone Encapsulant Crosslinker (Dow Corning, 4019862)
Silicon Wafer (University Wafer)
Spin Coater (Laurell Technologies Corporation, Model WS-400B-6NPP/LITE)
Hot Plate
100% Ethanol

Method:

1. Mix Sylgard 184 Silicone Encapsulant Base and Crosslinker at a 10:1 ratio in a 50 mL centrifuge tube manually for 15 min.
2. Centrifuged at 1000 rpm for 8 minutes to eliminate all gas bubbles in the mixture.
3. Pour the mixture onto a 100 mm silicon wafer and spin coated at 200 rpm for 1 minute.
4. Baked at 95° for 1 hour to catalyze the crosslinking reaction and allowed to sit for 24 more hours at room temperature to allow residual crosslinking to occur; store the membranes in 100% ethanol to remove any residual un-crosslinked polymers before being used to fabricate wrinkles.
5. Stretch the PDMS on the custom-built membrane stretcher to desired strain and leave in plasma chamber for 20 minutes to lower pressure enough for plasma production; treat at with plasma at the high setting (29.6 W) for desired amount of time.
6. Promptly remove stretcher when finished and release strain at desired rate. Store in 100% ethanol to remove unlinked oligomers.
7. Glue premade cast acrylic frame onto wrinkled substrate using PDMS and cure fully; ensure full seal to avoid media leakage.

Appendix B

Atomic Force Microscopy (AFM) Topography Protocol

Purpose: Atomic force microscopy measures the topography of the PDMS wrinkles, quantifying the wavelengths and amplitudes created by the plasma treatment.

Materials:
Atomic Force Microscopy system (Asylum Research AFM)
AFM aluminum-coated silicon tips (Oxford Instruments, AC240TSA-R3)
Igor Pro 6.37 AFM data acquisition software (WaveMetrics)
Gwyddion AFM data analysis software (Czech Metrology Institute)

Method:

Setup

1. Superglue sample of wrinkled PDMS to glass slide
2. Turn on light and laser
3. Start up IgorPro AFM Software
4. Go to Standard → Topography → Contact Mode

Tip Preparation

1. Insert AFM tip in to cantilever holder, aligning to be parallel with the base
2. Screw down until finger tight

AFM Head Preparation

1. Insert cantilever holder in to the AFM head
2. Activate camera
3. Use knobs to locate the cantilever, and the slot disk to focus on it
4. Move the laser onto the tip until the Sum is high, indicating laser is in correct position
5. Adjust PD to change Deflection to 0

Calibrate Probe

1. Go to Thermal → Get Real Probe
2. Select correct tip and calibrate
3. Observe spectral peak and confirm that peak is found
4. Check that spring constant is within range of selected tip

Positioning Tip onto Sample

1. Make sure head is level
2. Raise head about 5x revolutions of front wheel to raise the front up
3. Remove head
4. Secure glass slide with double sided tape on the stage
5. Reposition the head
6. Click Engage Tip
7. Lower tip until the Z value is approximately 75
8. Close the AFM chamber, set desired topography scanning parameters, and run
9. Scan at Scan Size = 4 nm ; Scan Rate = 0.25 Hz ; Points and Lines = 512 ; Set Point = 0.950 V
10. Set image to be saved in proper file, in '.ibw' format (IGORPro Binary Wave)
11. Raise head about 5x revolutions of front wheel to raise front up before removing head to take out sample

Reading Samples

1. Open Gwyddion software
2. Use 3DRetrace to see peak values and derive amplitude
3. Use Measure to manually measure wavelengths in image and derive mean

Appendix C

Primary Murine Neonatal Cardiomyocyte Culture Protocol

Purpose: Rat primary neonatal cardiomyocytes are isolated and digested in preparation for cell culture. Cell density is calculated via cell counting and are seeded at appropriate numbers on pre-treated substrate.

Materials:
2-day old Sprague-Dawley rat primary cardiomyocytes (Charles River Laboratories)
Dulbecco's Modified Eagle Medium (DMEM) 1X (Gibco, 11965-084)
Trypsin (Gibco, 25200-072)
Hank's Balanced Salt Solution (HBSS) (Gibco, 10425076)
L-15 Medium (Gibco, 11415064)

Plasma Cleaner
Human Plasma Fibronectin (EMD Millipore, FC010)
Phosphate Buffered Solution (PBS) 1X (Corning, 21-1040-CV)

Method:
Day 1

1. Prepared trypsin by dissolving into 2 mL with 1x HBSS
2. Put neonatal hearts into 25 mL HBSS on ice and wash them twice with 10 mL pipette
3. Pour the heart out, put in petri dish, and cut into very small pieces within solution
4. Refrigerate at 4°C for 20-24 hours

Day 2

1. Prepare trypsin inhibitor solution by mixing powder with 1 mL HBSS, using 0.5 mL for 10-12 hearts
2. Place heart pieces and solution in 50 mL tube
3. Add 0.5 mL trypsin inhibitor into tube and mix gently
4. Oxygenate tissue for 30-60 s by passing oxygen over the surface of the liquid
5. Place tube into 37°C water bath for 30 seconds
6. Add prepared collagenase 2 (300 U per 5 mL L-15 media)
7. Shake solution on shaker for 150 min, and check isolation results in process until no solid heart pieces seen
8. Use 10 mL pipette and flush 10 times
9. Filter solution through 70 μm pore size filter
10. Add 5 mL L-15 media to wash remains at bottom

11. Flush 10 times very gently
12. Filter through same film into same tube (should be 19.5 mL)
13. Oxygenate for 1 minute, pre-clean pipette with alcohol wipes
14. Place tube with filtered cells into hood at RT for 40 min; check frequently for clustering on bottom
15. Centrifuge solution at 800 rpm for 3 min
16. Resuspend cells very gently with 20 mL DMEM/ high glucose with 10 FBA until no apparent clusters of cells at bottom
17. Plate cells into two 100 mL culture dishes evenly spread and leave for 2 hours in
18. incubator
19. Remove solution and flush dishes 3x to obtain optimal density of cells
20. Add 10 mL media to wash out unattached cells
21. Count cells

Substrate Preparation:

1. Plasma treat wrinkled substrate with cast acrylic for 20 minutes to sterilize surface
2. Dilute fibronectin in sterile PBS at 11 μg/mL
3. Coat sterilized wrinkles with fibronectin solution in sterile hood for at least 4 hours to encourage cell adhesion
4. Rinse off excess fibronectin solution before seeding with DMEM
5. Add appropriate cell density to wrinkles and add supplemental DMEM as needed
6. Change media 24 hours after seeding and in 48 hour intervals subsequently

Appendix D

Cardiomyocyte Immunostaining Protocol

Purpose: Fixed cells undergo fluorescent staining for α-actinin to visualize structural maturity. Fluorescence images are analyzed using a customized Matlab program to output a coefficient of alignment.

Materials:
0.025% Triton X-100 (Sigma, 234729)
10% Normal Donkey Serum (NDS) (Sigma, D9663)
Monoclonal Anti-α-actinin mouse (Sigma, A2172)
Donkey anti-Mouse igG, Alexa Fluor 594 (Invitrogen, A11005)
Phosphate Buffered Solution (PBS) 1X (Corning, 21-1040-CV)
ProLong Gold Antifade Mountant with DAPI (Thermo Fisher, P36930)
EVOS Imaging System (Thermo Fisher)
Plan-APOCHROMAT 63x Oil Immersion Objective (Zeiss)
Immersol 518F Immersion Oil (Zeiss, 12-624-66A)
Cover slip
Microscope slide

Method:

Sample Prep

1. Dry off excess PBS from samples
2. Coat samples 0.25% Triton X-100 at room temperature
3. Wash with PBS 1x twice, 5 minutes each; use Kimwipe to dry off in between from the side (don't wipe samples directly!)
4. Coat samples with 10% Normal Donkey Serum and leave at RT for 1 hour

Primary Antibody

1. Dilute Monoclonal Anti-α-actinin mouse 1:400 in PBS 1x
2. Keep in fridge for 12 hours, protecting from light
3. Wash off primary antibody with 1x PBS thrice, 5 minutes each on stirrer; use Kimwipe to dry off in between from the side

Secondary Antibody

1. Dilute Alexa Fluor 594 1:200 in PBS 1x

2. Add to samples and keep in fridge for 12 hours
3. Wash off secondary antibody on stirrer with PBS 1x thrice, 15 minutes each; use Kimwipe to dry off in between from the side

Prepare Sample for Imaging

1. Drop ProLong Mountant with DAPI onto cover slip
2. Carefully cut out sample and place facedown on mountant
3. Seal with microscope slide
4. Keep away from light!

Imaging

1. Turn on EVOS Imaging System
2. Make sure Zeiss 63x objective is in position
3. Cover objective in Immersol oil and make sure it is pulled down to avoid collision with sample
4. Place sample cover slip-side down and cover with light shield to prevent photobleaching
5. Locate cells in correct field of view using bright light mode
6. Image DAPI and α-actinin using appropriate excitation wavelengths
    a. DAPI:
    b. α-actinin:
7. Save data in .tif file format

Appendix E

Fluo-4 Calcium Cycling Protocol

Purpose: Fluo-4 is a dye that binds to calcium *in vivo*, allowing for visualization of calcium ion transport in cardiomyocytes under fluorescence.

Materials:
Fluo-4, AM 1000X in DMSO (Invitrogen, F10489)
PowerLoad Concentrate, 100X (Invitrogen, F10489)
Probenecid (Invitrogen, F10489)
Tyrode's Salts without Sodium Bicarbonate (HiMedia, TS1012)
Sodium Bicarbonate (Sigma, S5761)
PBS 1X (Corning, 21-1040-CV)

Function Generator (Techtronix, AFG1062)
Oscilloscope (Techtronix, TDS 2014)
AxioVision software (Carl Zeiss)
Carbon Electrodes (GSC International, 505-1)
AxioSkop 2 Plus Microscope (Carl Zeiss)
LUMPlanFL60x Water Immersion Objective (Olympus Life Sciences)

Method:
Tyrode's Solution Preparation

1. Add Tyrode's Salts to 1 L of PBS 1X and use magnetic stirrer to dissolve (How much SB?)

Fluo-4 Preparation

1. To prepare Fluo-4 AM Loading Solution, add 100 µL of 100X PowerLoad concentrate and 10 µL of Fluo04, AM 1000X to a 15 mL tube
2. Vortex to mix
3. Add 10 mL of Tyrode's Solution and invert tube to mix

Fluo-4 Loading

1. Remove media from cell sample and wash cells once with PBS 1X
2. Dilute above Fluo-4 preparation 2:1 with warmed Tyrode's Solution 1X in 1 mL aliquot
3. Add 1 mL of this Fluo-4 diluted solution and place sample into light-proof container
4. Incubate cells for 15 minutes at 37°C, followed by 15 minutes at room temperature
5. Remove Fluo-4 solution and wash cells once with warmed PBS 1X
6. Add Tyrode's solution and incubate cells for 20 more minutes at 37°C

Imaging

1. Turn on halogen light for 5 minutes to allow to warm up
2. Use 494 nm light to excite cells, which will emit at 506 nm
3. Set function generator to biphasic 5V at 1 Hz for 50 ms long; attach carbon rods
4. Place sample on glass microscope slide and on stage
5. Lower 60x Water Immersion Objective, observing through eyepiece until cells are in focus
6. Place carbon rod electrodes on either side of objective lens submerged in solution
7. Validate through eyepiece that stimulation causes cells to beat
8. Turn on fluorescence
9. Observe cycling of calcium

Data Acquisition

1. Open Multidimensional Acquisition, select Time Lapse, and set these parameters constant:
    a. Exposure = 100 ms (fixed)
    b. Duration = 10 s
    c. Interval Settings = Maximal Speed
    d. Dye = Fluo-4
2. Set correct file save path
3. Change from eyepiece to camera and confirm optimal focus
4. Click start to record data
5. Save as .tif images

Data Analysis

1. Use ImageJ to open .tif files of sequence and convert to stack
2. Manually trace each cell's outline and measure fluorescence intensity
3. Export data to Excel
4. Convert frame number to time in seconds and intensity into F/F_0
5. Plot this data to observe changes in calcium intensity over time